Check for updates

Received: 26 September 2025 | Revised: 31 March 2026 | Accepted: 15 April 2026

DOI: 10.1002/qj.70215

Quarterly Journal of the Royal Meteorological Society RMetS

RESEARCH ARTICLE

Observations and numerical simulations of a valley-exit wind in the Alpine Bolzano basin

Federica Gucci[1,2] | **Andrea Zonato**[2,3] | **Marco Falocchi**[2,4] | **Dino Zardi**[2,5] | **Lorenzo Giovannini**[2]

[1]Institute of Geophysics and Meteorology, University of Cologne, Cologne, Germany

[2]Department of Civil, Environmental and Mechanical Engineering, University of Trento, Trento, Italy

[3]CIMA Research Foundation, Savona, Italy

[4]CISMA S.r.l., Bolzano, Italy

[5]Center Agriculture Food Environment (C3A), University of Trento, Trento, Italy

Correspondence
Federica Gucci, Institute of Geophysics and Meteorology, University of Cologne, Cologne, Germany.
Email: fgucci@uni-koeln.de
Lorenzo Giovannini, Department of Civil, Environmental and Mechanical Engineering, University of Trento, Trento, Italy.
Email: lorenzo.giovannini@unitn.it

Abstract

The characteristics of the nocturnal drainage wind flowing from the tributary Isarco Valley into the Bolzano basin, in the Italian Alps, during wintertime are investigated. Analyses are performed by combining measurements from an intensive field campaign and the output of four high-resolution numerical simulations, run with the Weather Research and Forecasting (WRF) model using different planetary boundary-layer (PBL) schemes. Two episodes are identified, based on the vertical temperature stratification in the basin and the evolution of the drainage flow at the valley exit. Numerical results show that the drainage flow behaves as a valley-exit wind, the main structure of which at the exit of the valley is captured well by the model independently of the PBL scheme. However, the model struggles to reproduce the temperature stratification in the basin correctly, with better results when a PBL scheme including, among others, a prognostic equation for the temperature variance and a counter-gradient term is used. This has an impact on the simulation of the onset and duration of the valley-exit wind, which are sensitive to the temperature contrasts between the valley and the basin. Overall, the model is able to reproduce the different behavior of the drainage wind at the exit of the valley in the two case studies. It is found that the presence of a cold-air pool in the basin favors an upward trajectory of the flow at the exit of the valley, resulting in unperturbed calm wind conditions in the lower levels. On the other hand, with weak temperature stratification, the drainage flow follows the topography closely, also resulting in strong winds near the surface.

KEYWORDS

Bolzano basin, cold-air pool, complex terrain, stable boundary layer, valley-exit wind, WRF model

This is an open access article under the terms of the Creative Commons Attribution License, which permits use, distribution and reproduction in any medium, provided the original work is properly cited.
© 2026 The Author(s). *Quarterly Journal of the Royal Meteorological Society* published by John Wiley & Sons Ltd on behalf of Royal Meteorological Society.

1 | INTRODUCTION

Almost half of the Earth's land surface is covered by hilly or mountainous terrain (Meybeck *et al.*, 2001). Hence, the understanding of atmospheric circulations over these regions is an important issue for many sectors, including weather forecasting, pollutant dispersion, and renewable energy source assessment. However, atmospheric circulations over mountainous regions are much more complex than over flat terrain, due to the interaction between the flow and the orography at different spatial and temporal scales (Adler *et al.*, 2021; Babić *et al.*, 2021; Lapo *et al.*, 2025; Lehner & Rotach, 2018).

Under fair weather conditions, different types of thermally driven circulations typically develop over mountain regions (Zardi & Whiteman, 2013), driven by pressure gradients produced by differential heating of the atmosphere in adjacent areas. In particular, mountain valleys are affected by the development of cross- and along-valley circulations, generally called slope and valley wind systems, respectively (Giovannini *et al.*, 2017; Rucker *et al.*, 2008; Schmidli *et al.*, 2009; Whiteman, 1990).

When the surface energy budget results in radiative loss, the near-surface atmospheric layer becomes stably stratified, reducing vertical motion and turbulent mixing. Thermally driven down-valley and down-slope flows may contribute, through convergence from tributary valleys and sidewalls, to strengthening the stratification of the valley atmosphere, with the development of strong thermal inversions and cold-air pool (CAP) episodes (De Wekker & Whiteman, 2006). CAPs consist of a topographically confined, stagnant layer of air close to the surface colder than the atmosphere above (Whiteman *et al.*, 2001). CAPs typically form in local depressions and valley constrictions (Clements *et al.*, 2003; Lundquist *et al.*, 2008) during the evening/night and break up after sunrise of the next day, due to the energy input provided by solar radiation and the consequent surface heating. However, especially during wintertime and in mountain areas, the CAP can persist for several days, due to the weaker solar radiation input, also determined by mountain shading (Clements *et al.*, 2003; Daly *et al.*, 2009; Lareau *et al.*, 2013a; Lundquist *et al.*, 2008; Rauchöcker *et al.*, 2024).

There is a mutual interaction between the local airflow and the CAP. Convergence of down-slope flows contributes to increasing the depth of the CAP until the down-valley flow is fully developed. Once a CAP has formed, it may, in turn, influence the local circulation. A deep stable layer, in fact, may act as a material surface (sometimes referred to as an *effective mountain*) to the airstream impinging on it (Lin *et al.*, 2005; Muñoz *et al.*, 2020; Neff & King, 1987, 1989; Reeves & Lin, 2006). Numerical simulations have shown that down-slope winds may split when they reach the cold air accumulated inside a basin, flowing partly close to the surface and partly above the CAP (Cuxart *et al.*, 2007). On the other hand, the presence of flows on top of the CAP may contribute to its erosion by shear-driven turbulence at the interface (Lareau & Horel, 2015), a process that was shown to be non-negligible, especially for CAP erosion by föhn (Haid *et al.*, 2022; Jaubert *et al.*, 2005).

The present work focuses on a nocturnal drainage current flowing from a tributary valley into the basin of Bolzano (Italian Alps) during wintertime. The formation of a CAP in the basin is expected to alter the spatial characteristics of the current, which are investigated under two distinct temperature stratifications in the basin, combining measurements from an intensive field campaign and results from numerical simulations with the Weather Research and Forecasting (WRF) model. Meteorological data were collected during the Bolzano Tracer EXperiment (BTEX) in January and February 2017 (Falocchi *et al.*, 2020; Tomasi *et al.*, 2019; Zardi *et al.*, 2021), providing both surface measurements and vertical profiles of temperature, wind speed, and direction. These experimental data serve both to characterise local meteorological conditions, in particular the drainage wind, and to evaluate model results. The representation of very stable planetary boundary layers (PBLs) with numerical models is challenging, due to the reduced and intermittent turbulent mixing (Boyko & Vercauteren, 2024; Sandu *et al.*, 2013). This, combined with the complex topography where CAP generally occurs and the many atmospheric processes that shape its evolution and structure (Lareau *et al.*, 2013b), makes it even more difficult to represent such a phenomenon (Adler *et al.*, 2023; Arthur *et al.*, 2021) and makes the model more sensitive to the representation of the PBL dynamics (Ma *et al.*, 2024). For this reason, the performance of four different PBL schemes in reproducing the evolution of the drainage flow once it reaches the basin is assessed. Among the PBL schemes tested, a new scheme including a prognostic equation for turbulent potential energy (TPE) is adopted, since it is known that the conversion between turbulent kinetic energy (TKE) and TPE is a crucial mechanism in stable boundary-layer dynamics (Zilitinkevich *et al.*, 2007). While this new scheme has been evaluated in idealised simulations of mountain environments (Zonato *et al.*, 2022), it is tested for the first time here in real-case complex-terrain scenarios.

Based on model verification results, a simulation for each episode is then selected to provide a more complete analysis of the spatial development of the drainage flow and its interaction with the air in the Bolzano basin, complementing the punctual information from the experimental measurements. The first insights from the BTEX experiment had shown that the nocturnal drainage current

1477870x, 0, Downloaded from https://rmets.onlinelibrary.wiley.com/doi/10.1002/qj.70215 by Lorenzo Giovannini - Universita Di Trento , Wiley Online Library on [07/05/2026]. See the Terms and Conditions (https://onlinelibrary.wiley.com/terms-and-conditions) on Wiley Online Library for rules of use; OA articles are governed by the applicable Creative Commons License

presents characteristics similar to valley-exit jets (Tomasi *et al.*, 2019) and the numerical simulations will be used to confirm this hypothesis. Also, the interaction of CAP events with strong flow is a complex process that cannot be captured fully by point measurements. Therefore, the results of the numerical simulations are used to understand how the formation of a CAP affects the spreading of the valley-exit wind into the basin. While several observational and numerical studies have been conducted to investigate CAP processes (Arduini *et al.*, 2016; Clements *et al.*, 2003; Price *et al.*, 2011; Rauchöcker *et al.*, 2024), only a few have analysed the interaction with the local circulation, focusing mainly on föhn events (Flamant *et al.*, 2006; Haid *et al.*, 2020; Umek *et al.*, 2021), rather than smaller-scale flows, such as valley-exit jets.

Valley-exit jets are a specific type of low-level jet (LLJ: Banta *et al.*, 1996, 2007; Stensrud, 1996; Chrust *et al.*, 2013; Tuononen *et al.*, 2017; Nikolic *et al.*, 2019; Svensson *et al.*, 2019) that have been documented at canyon (Banta *et al.*, 1995; Chrust *et al.*, 2013; Muñoz *et al.*, 2020) or valley exits (Drobinski *et al.*, 2006; Hellström *et al.*, 2017; Jiménez *et al.*, 2019; Pamperin & Stilke, 1985; Pfister *et al.*, 2024; Sasaki *et al.*, 2010; Spengler *et al.*, 2009), where topography changes abruptly, opening onto a basin or a plain. They often arise as a local modification of down-valley flows, and occur during nights with weak synoptic forcing and clear sky. Hydraulic theory and transition of the flow from a subcritical to a supercritical state explain the basic dynamics: a deep layer of cold air drains out of the canyon/valley, sinks, and compresses, accelerating downward into a shallower layer forming the jet, with an increase in wind speed caused by the conversion of potential into kinetic energy (Chrust *et al.*, 2013; Muñoz & Armi, 2024). This conversion mechanism was observed at the exit of the Inn Valley (Zängl, 2004), where the flow reached its maximum intensity ($15\,m{\cdot}s^{-1}$ at a height of 200 m above ground level, AGL) close to sunrise. Surface friction at the sidewalls may contribute to shaping the structure of the jet. The release from the frictional effects at the valley exit contributes to the acceleration of the down-valley flow (Banta *et al.*, 1995) and the approximate conservation of potential vorticity generated at the sidewalls leads the flow to maintain its shape beyond the exit region (Zängl, 2004).

The interplay of these mechanisms shapes the valley-exit flow and its interaction with the basin air, creating a complex flow structure. Consequently, high-resolution numerical simulations are essential to investigate its propagation into the basin. The simulations performed for this work aim to answer the following research questions: does the drainage flow behave as a valley-exit wind? Is the simulation of the thermal conditions in the basin and of the valley-exit wind sensitive to the PBL scheme? How is the valley-exit wind affected by the development of a CAP in the basin? Does the valley-exit wind flow close to the ground in the basin, split, or flow above the CAP?

The article is organised as follows. Section 2 describes the area of interest and the BTEX experiment, together with the two case studies. Section 3 focuses on the setup and initialisation of the sub-kilometer numerical simulations. Results are presented in Sections 4 and 5. In Section 4 a qualitative as well as quantitative evaluation of the model performance with the different PBL schemes is provided, and in Section 5 the spatial structure of the drainage flow is investigated, as well as the interaction between the drainage flow and the air in the Bolzano basin. Finally, conclusions are drawn in Section 6.

2 | STUDY AREA AND EXPERIMENTAL MEASUREMENTS

2.1 | The Bolzano basin

The city of Bolzano (254 m above sea level, a.s.l.) lies in the Adige Valley, in the northeastern Italian Alps. Here, the valley widens into a basin-like area and joins with two tributary valleys: the Sarentina Valley from the north and the Isarco Valley from the east. The heights of the mountain crests surrounding the basin range between 1200 and 2000 m a.s.l. (Figure 1). The Isarco Valley is a V-shaped valley, with a very narrow valley floor close to its exit onto the Bolzano area and a dominant southwest–northeast orientation, although it includes several bends along its length (about 80 km). During night-time, a ground-based temperature inversion occurs frequently in the Bolzano basin under weak synoptic forcing and clear-sky conditions. It starts building up in the late afternoon and ends some hours after sunrise, when the energy input from solar radiation is sufficient to break up the inversion layer. The formation of a CAP in the basin, which interacts with the local circulation, is crucial for pollutant dispersion processes in the area, where significant emissions due to traffic, domestic heating and industrial activities are present (Bisignano *et al.*, 2022), contributing to frequent poor air quality conditions.

2.2 | BTEX experiment

BTEX took place in winter 2017 to study the dispersion of pollutants from a waste incinerator, located 2 km southwest of the city of Bolzano (Falocchi *et al.*, 2020; Zardi *et al.*, 2021). During BTEX, multiple instruments were used to monitor atmospheric conditions in the area,

1477870x, 0, Downloaded from https://rmets.onlinelibrary.wiley.com/doi/10.1002/qj.70215 by Lorenzo Giovannini - Universita Di Trento , Wiley Online Library on [07/05/2026]. See the Terms and Conditions (https://onlinelibrary.wiley.com/terms-and-conditions) on Wiley Online Library for rules of use; OA articles are governed by the applicable Creative Commons License

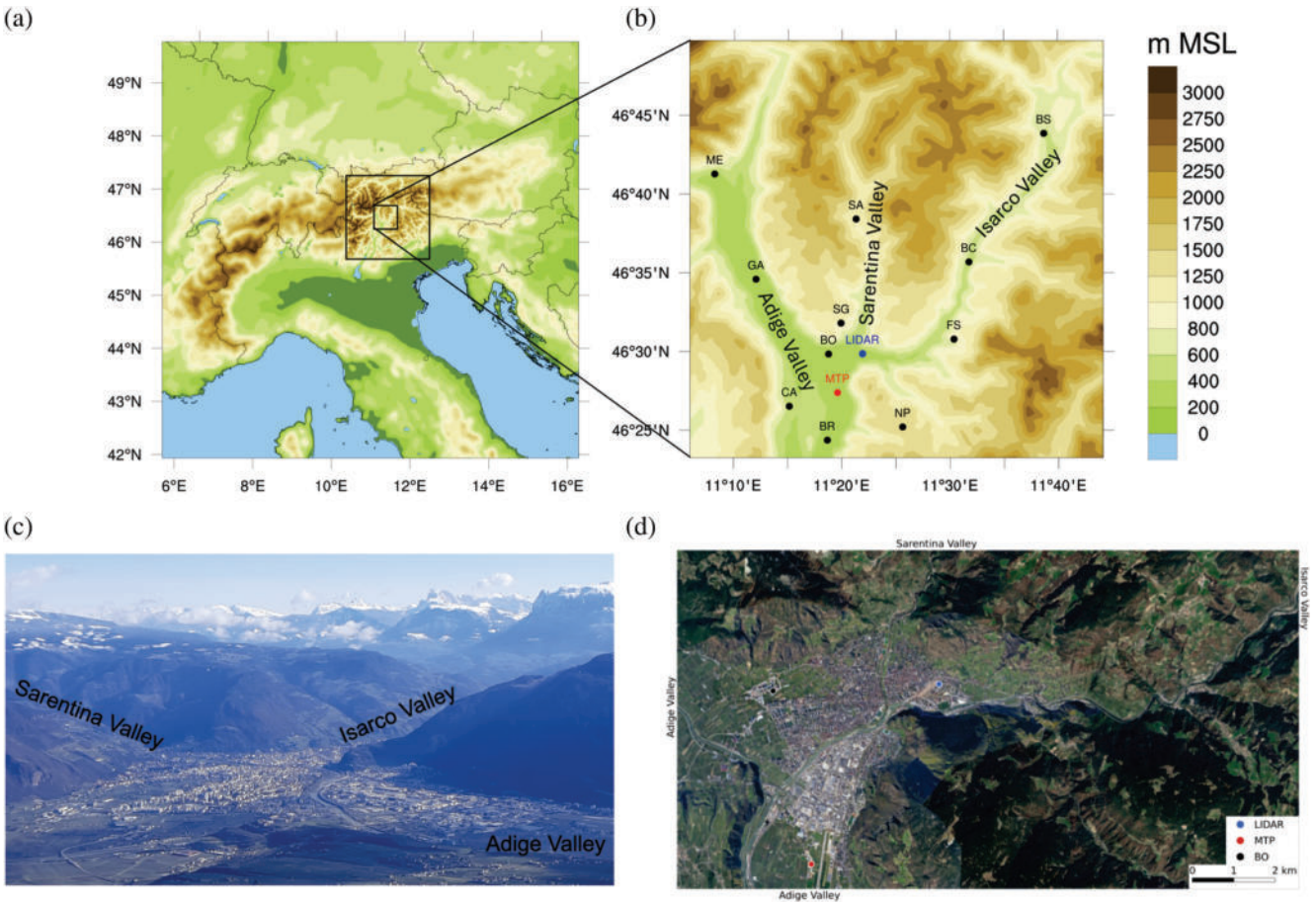


FIGURE 1 Area of study: (a) map of the three nested domains used for the WRF simulations and (b) zoom-in the innermost domain, with the locations of the instruments used to evaluate model results, that is, lidar, temperature profiler (MTP), and 11 ground weather stations (BR: Bronzolo, BO: Bolzano, GA: Gargazzone, ME: Merano, BC: Barbiano-Colma, CA: Caldaro, BS: Bressanone, FS: Fié allo Sciliar, SA: Sarentino, SG: San Genesio, NP: Nova Ponente). (c,d) Photo and aerial photo of the basin and the city of Bolzano with mountain crests surrounding the basin.

including a Doppler wind lidar, a thermal profiler, and 15 ground weather stations (GWSs). The Doppler wind lidar, a WINDCUBE 100S manufactured by Leosphere (France), was installed on the roof of a building close to the exit of the Isarco Valley. It provided vertical profiles of the wind along 106 vertical levels, 10-m spaced (from 335–1385 m a.s.l.) and with a vertical resolution of 25 m, averaged over 10 min. The temperature profiler, a MTP-5HE passive microwave radiometer manufactured by ATTEX (Russia), was operated by the Environmental Protection Agency of the Province of Bolzano and installed south of the city at the local airport, providing temperature measurements every 10 min and interpolated along 21 vertical levels, 50-m spaced (from 250–1250 m a.s.l.). GWSs were operated by the Meteorological Office of the Province of Bolzano. In this work, 11 out of 15 GWSs are used, because two are located outside our domain of interest and two were not working during the selected case studies. The GWSs provide 10-minute average data and are distributed quite homogeneously over the area, covering different heights from 226–1470 m a.s.l.. Further information on the measurement setup can be found in Falocchi *et al.* (2020), while a map with their location is shown in Figure 1b.

2.3 | Case studies

In order to identify suitable case studies, an analysis of the thermal stratification in the basin, together with near-surface wind conditions, is conducted for the months of January and February 2017.

Figure 2a,b shows the hourly temperature differences, for January and February 2017, between the measurements recorded by the temperature profiler at 450 and 250 m a.s.l. (200 m AGL and the surface), with red colors corresponding to temperature inversions in the basin. While persistent CAPs are not observed, nocturnal ones occur frequently, especially in January. Comparing this

1477870x, 0, Downloaded from https://rmets.onlinelibrary.wiley.com/doi/10.1002/qj.70215 by Lorenzo Giovannini - Universita Di Trento , Wiley Online Library on [07/05/2026]. See the Terms and Conditions (https://onlinelibrary.wiley.com/terms-and-conditions) on Wiley Online Library for rules of use; OA articles are governed by the applicable Creative Commons License

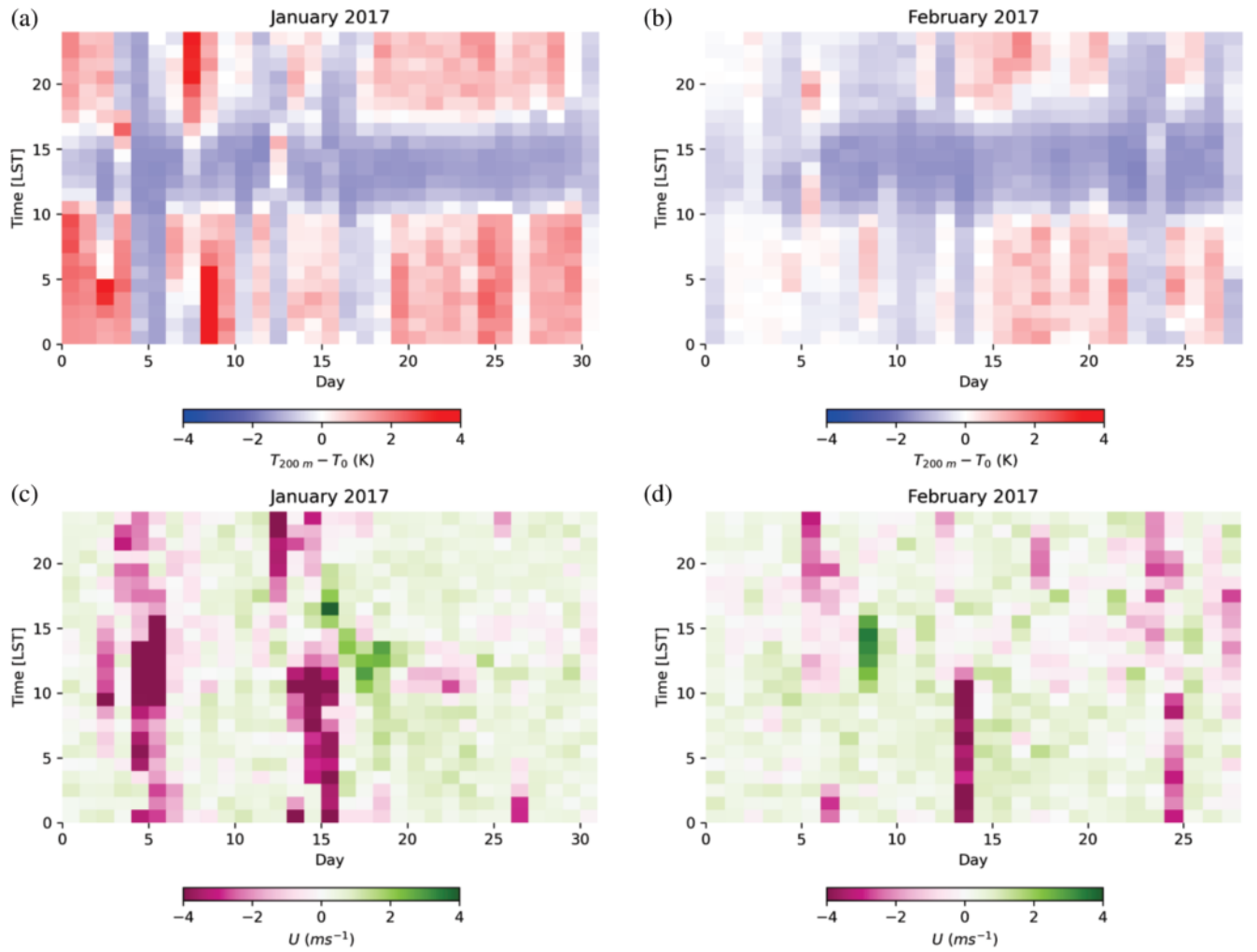


FIGURE 2 Monthly evolution of hourly temperature differences between 450 and 250 m a.s.l. (200 m AGL and the surface) from temperature profiler measurements in (a) January and (b) February. Monthly evolution of the hourly west–east component of the 10-m wind speed measured at Bolzano GWS (see Figure 1b) in (c) January and (d) February.

situation with the west–east component of the 10-m wind speed measured at Bolzano GWS (Figure 2c,d), it can be observed that easterly winds (pink values) during night-time are generally registered when no temperature inversion or a weak stratification is present in the basin.

On the other hand, when a strong inversion builds up, westerly winds are generally observed during night-time at Bolzano GWS. In February (Figure 2d), easterly winds are rarely observed at the ground, and the night between February 13 and 14 appears to be an exceptional case of strong easterly wind, again occurring when a thermal inversion is not present in the basin. This night and the night between January 28 and 29 (also considering that wind lidar measurements are available from January 9, Falocchi *et al.*, 2019) are selected as case studies. These two case studies allow us to analyse the interaction between the valley-exit wind of the Isarco Valley and the air in the Bolzano basin in two opposite situations, that is, when a strong CAP is present (January 28–29, Episode 1) and without a CAP (February 13–14, Episode 2).

In the January 28–29, 2017 case, northern Italy was under a high-pressure system with no appreciable synoptic winds and the area of Bolzano was cloud-free.

The February 13–14, 2017 episode was similarly characterised by high-pressure conditions over northern Italy, but in this case weak southeasterly synoptic winds transported moisture from the Mediterranean towards the Alps, as evidenced by an increase in absolute humidity recorded by many GWSs at varying altitudes (see fig. 6c in Falocchi *et al.*, 2020). As a consequence, stratocumulus clouds were present above the Adige Valley during the night, hindering radiative cooling and the consequent formation of a ground-based temperature inversion in the basin. Satellite images show that clouds were restricted to the Adige Valley and the Bolzano basin, leaving the Isarco Valley cloud-free and leading to a strong thermal gradient

1477870x, 0, Downloaded from https://rmets.onlinelibrary.wiley.com/doi/10.1002/qj.70215 by Lorenzo Giovannini - Universita Di Trento , Wiley Online Library on [07/05/2026]. See the Terms and Conditions (https://onlinelibrary.wiley.com/terms-and-conditions) on Wiley Online Library for rules of use; OA articles are governed by the applicable Creative Commons License

between the tributary valley, with cooler air, and the basin, with the development of a nocturnal down-valley flow.

3 | MODEL SETUP

Simulations are performed with WRF model version 4.3.3 (Skamarock *et al.*, 2019). Each simulation lasts 42 hours and starts the day before the night of interest (January 28, 0000 UTC for Episode 1 and February 13, 0000 UTC for Episode 2). The first 14 hours are considered spin-up time. Three two-way nested grids are used (Figure 1a) with 196^2, 196^2, 166^2 horizontal cells (Δx =4.5, 0.9, 0.3 km), while 61 levels are used in the vertical direction, with 24 levels below 1000 m AGL and the first model level at 14 m AGL. The inner domain covers the area of interest (Figure 1b).

Four simulations for each episode are performed, with the following choices of PBL scheme:

1. Yonsei State University (YSU: Hong *et al.*, 2006),
2. Mellor–Yamada–Janjic (MYJ: Janjic, 2002),
3. Bougeault–Lacarrére (BouLac: Bougeault & Lacarrére, 1989), and
4. a k–ϵ-based closure recently proposed in Zonato *et al.* (2022) (KEPS-TPE).

The YSU PBL scheme is a first-order closure, while MYJ and BouLac are 1.5-order closures with a prognostic equation for the TKE, with MYJ based on Mellor (1982) (level 2.5) and BouLac on Therry and Lacarrére (1983). The KEPS-TPE PBL scheme is a k–ϵ-based closure, including prognostic equations for the TKE, its dissipation rate, and the temperature variance. The latter is directly connected to the TPE. The heat-flux parameterisation includes a counter-gradient term proportional to the temperature variance and accounts for the self-control mechanism of stratified turbulence (Zilitinkevich *et al.*, 2007). YSU, BouLac, and KEPS-TPE are coupled to the MM5 surface-layer scheme (Grell *et al.*, 1994) and MYJ to the MYJ Eta scheme (Janjić, 1994) to calculate surface–atmosphere exchange.

The microphysics scheme adopted is WRF Single-Moment 6-Class Microphysics Scheme (WSM6) (Hong & Lim, 2006), while the WRF Rapid Radiative Transfer Model (RRTM) scheme (Mlawer *et al.*, 1997) is used for long-wave radiation and the Dudhia (1989) scheme for short-wave radiation, including the effects of slope inclination and topographic shading. No cumulus parameterisation is used in any of the domains, but the microphysics scheme was activated to reproduce the stratocumulus clouds observed in the valley in Episode 2. The land-surface model (LSM) adopted is Noah-MP (Niu *et al.*, 2011).

Meteorological data from the ECMWF Reanalysis Version 5 (ERA5) released by the European Centre for Medium-Range Weather Forecasts (ECMWF) are used as initialisation and lateral boundary conditions every 6 hours, with a horizontal resolution of ∼ 30 km on 137 vertical atmospheric levels and at the surface. Several preliminary simulations were performed in order to improve the initial surface conditions. It is well known that increasing the spatial resolution of simulations without incorporating improved surface data does not automatically imply an improvement of the model performance (Chow *et al.*, 2006). In particular, attention was paid to soil moisture and snow cover, which influence the development of thermally driven circulations and the near-surface stratification (Banta & Gannon, 1995; Jiménez *et al.*, 2019; Massey *et al.*, 2016; Ookouchi *et al.*, 1984; Tomasi *et al.*, 2017).

ERA5 overestimates snow cover for both case studies, with snow cover even inside the Adige Valley, which was not present. On the basis of photographs taken during the field campaign, the snow cover was limited to heights above 2000 m MSL. With this modification alone, a deep-frozen soil layer formed on the first night of the simulation and did not melt during the day. This was attributed to poorly constrained soil variables in the initialisation—among others, soil temperature, which is expected to be close to freezing point on soil covered by snow. To introduce temporal and spatial variability in soil temperature, the conditional statement in the land-surface model that sets a grid point to freeze was forced never to be satisfied. While this is a compromise between two unrealistic soil physics conditions, this modification produced a more realistic distribution of the soil temperature, especially in valleys, and lower soil temperatures above 2000 m MSL. At those heights, a deep snow layer isolates the soil from the atmosphere above, thus the lower soil temperatures are expected not to impact the near-surface air temperature at those heights. Concerning soil moisture, unfortunately no in situ observations were available to improve model initialisation. Therefore, observations from the National Aeronautics and Space Administration (NASA) Soil Moisture Active Passive mission (SMAP),[1] with a horizontal resolution of 9 km, were adopted to obtain representative values of soil moisture in the area. For Episode 1, the comparison between SMAP soil moisture values and model initialisation suggested halving ERA5 soil moisture. A similar overestimation was found in Giovannini *et al.* (2014) in the Adige Valley. For Episode 2, in contrast, no adjustment was needed.

High-resolution topography data were obtained from the Viewfinder Panoramas website[2] with a spatial resolution of 1 arcsec (∼ 30 m) and smoothed slightly to prevent numerical instability. Similarly, the Corine Land Cover (CLC) dataset updated to 2012, provided by the European Environment Agency,[3] with a spatial resolution of

1477870x, 0, Downloaded from https://rmets.onlinelibrary.wiley.com/doi/10.1002/qj.70215 by Lorenzo Giovannini - Universita Di Trento , Wiley Online Library on [07/05/2026]. See the Terms and Conditions (https://onlinelibrary.wiley.com/terms-and-conditions) on Wiley Online Library for rules of use; OA articles are governed by the applicable Creative Commons License

100 m, was employed as land-use dataset after a proper reclassification of CLC classes into the 20 MODIS classes adopted by WRF, following Giovannini *et al.* (2014).

4 | PBL SCHEME INTERCOMPARISON

4.1 | January 28–29, 2017: Episode 1

Figure 3 shows the time–height plots of temperature from the thermal profiler and the simulations for Episode 1. An inversion layer started to build up a few hours after sunset (local sunset around 1600 LST), reaching a top height of 700 m AGL during the night, with a strong stratification close to the surface. The ground-based temperature inversion persisted for some time after sunrise (local sunrise around 1000 LST) before being eroded from the lowest atmospheric layers.

While none of the PBL schemes is able to reproduce the depth of the CAP, the KEPS-TPE PBL scheme aligns most closely with observations, yielding the coldest near-surface temperatures. This behavior is attributed to the counter-gradient term included in the scheme. By

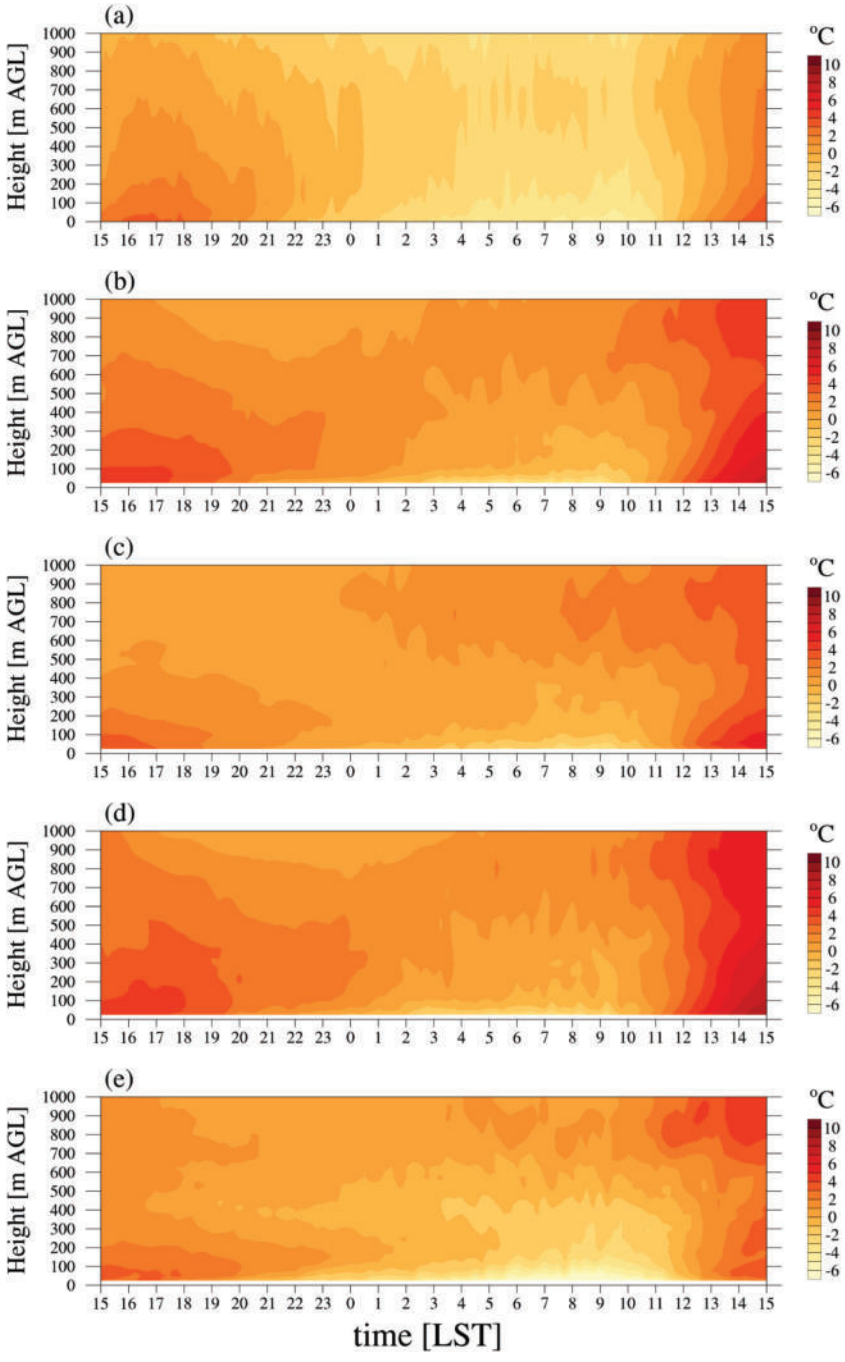


FIGURE 3 Time–height plots of temperature for Episode 1 at the temperature profiler site as (a) measured, and simulated by (b) YSU, (c) MYJ, (d) BouLac, and (e) KEPS-TPE.

1477870x, 0, Downloaded from https://rmets.onlinelibrary.wiley.com/doi/10.1002/qj.70215 by Lorenzo Giovannini - Universita Di Trento , Wiley Online Library on [07/05/2026]. See the Terms and Conditions (https://onlinelibrary.wiley.com/terms-and-conditions) on Wiley Online Library for rules of use; OA articles are governed by the applicable Creative Commons License

counteracting the purely local (down-gradient) diffusive component, this term weakens the coupling between the lowest layers and the atmosphere aloft. Consequently, this reduces downward heat transport, specifically the replenishment of warmer air from the residual layer toward the surface layer.

The time–height plots of the observed wind speed and direction at the lidar location (Figures 4a and 5a) highlight that the drainage (easterly) flow started to develop around 1900 LST after the formation of the thermally stable layer near the surface. The wind speed became continuously stronger over an increasingly deep layer up to a height of 900 m AGL, following the evolution of the thermal structure into the basin. Peaks in wind speed were reached in the morning at 0800 LST below 400 m AGL, with an intensity of $\sim 10\ \mathrm{m \cdot s^{-1}}$. Then the drainage flow died out rapidly, starting from the surface. All PBL schemes reproduce the onset of the drainage wind exiting

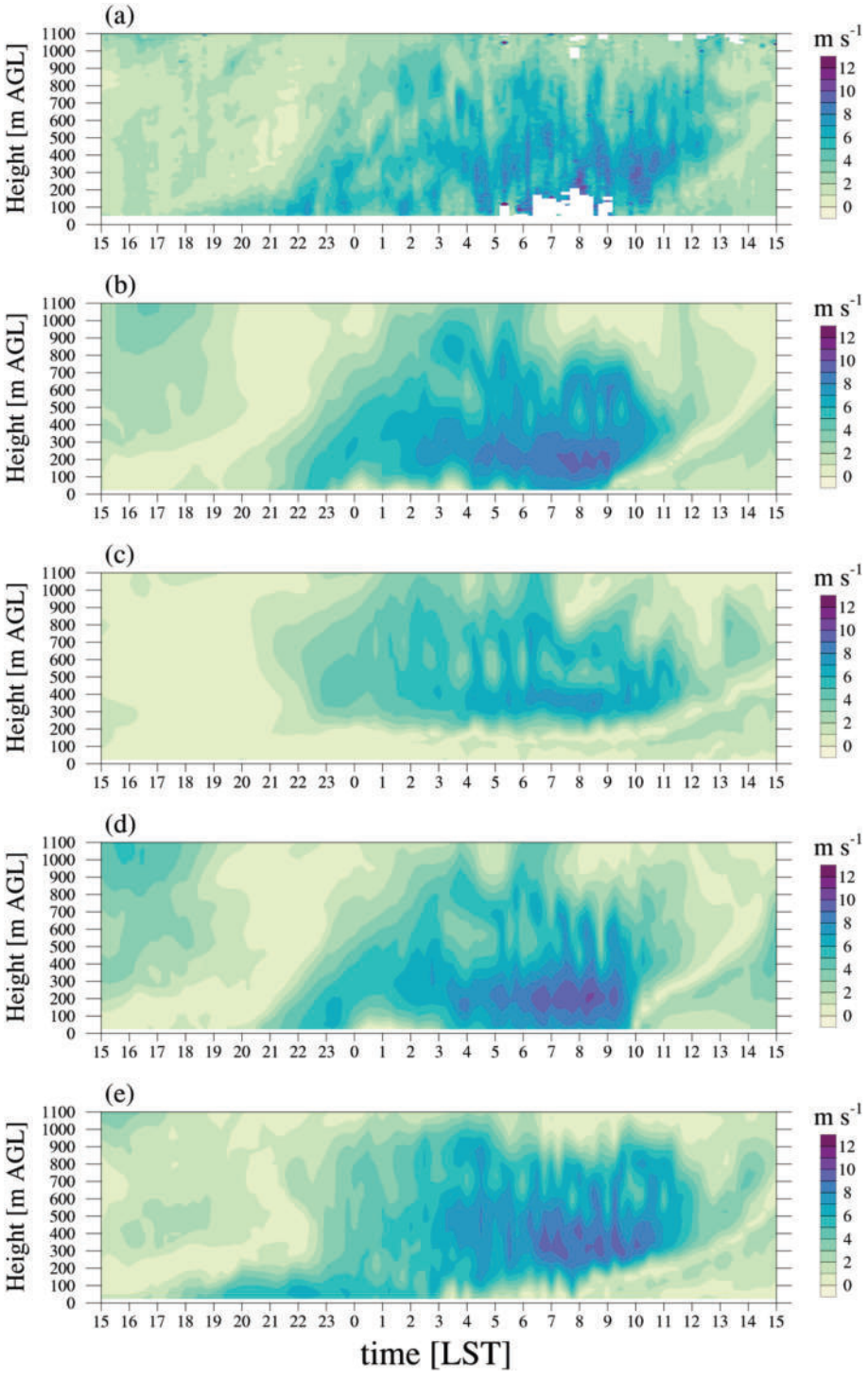


FIGURE 4 Time–height plots of horizontal wind speed for Episode 1 at the lidar site as (a) measured, and simulated by (b) YSU, (c) MYJ, (d) BouLac, and (e) KEPS-TPE.

1477870x, 0, Downloaded from https://rmets.onlinelibrary.wiley.com/doi/10.1002/qj.70215 by Lorenzo Giovannini - Universita Di Trento , Wiley Online Library on [07/05/2026]. See the Terms and Conditions (https://onlinelibrary.wiley.com/terms-and-conditions) on Wiley Online Library for rules of use; OA articles are governed by the applicable Creative Commons License

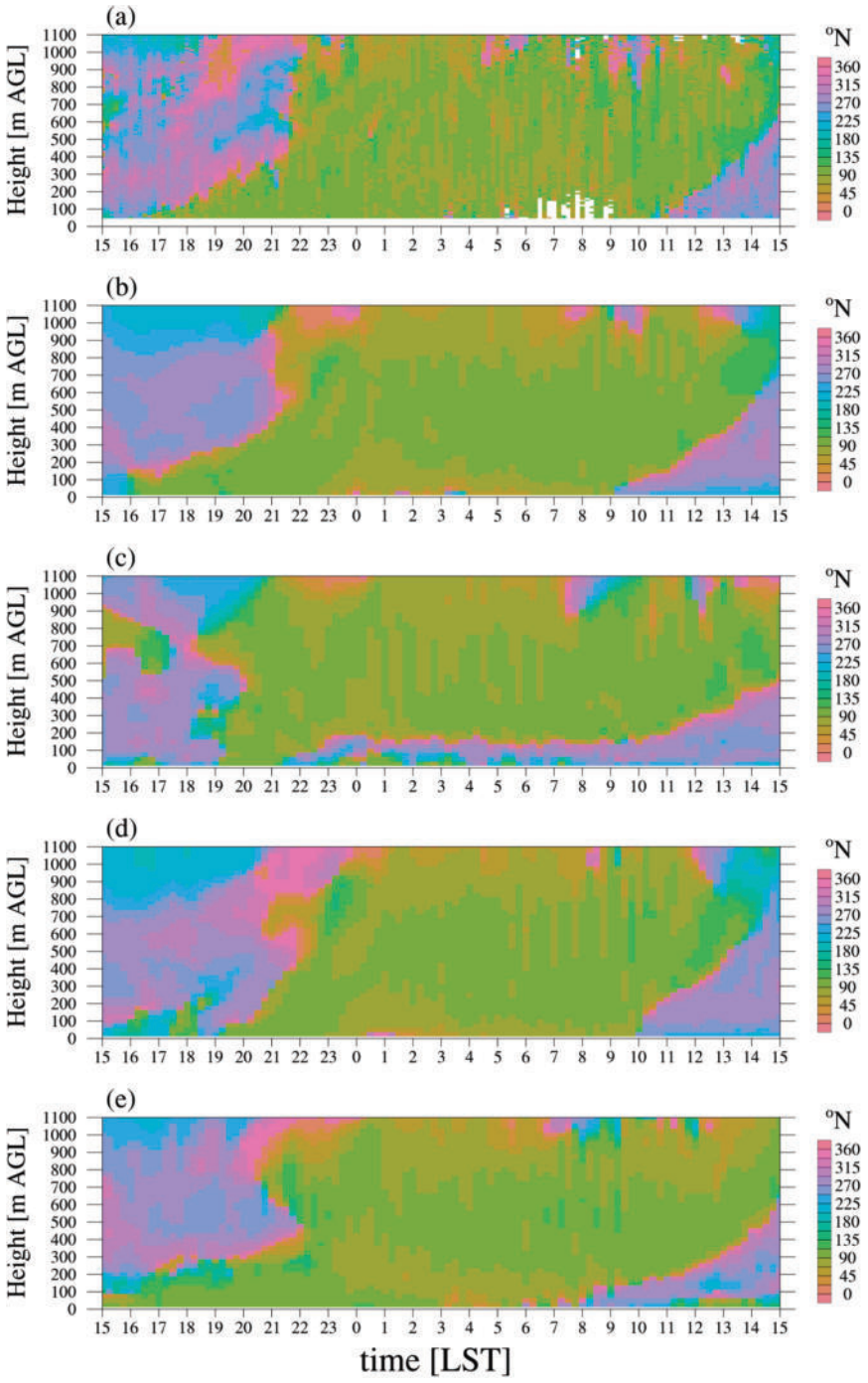


FIGURE 5 Time–height plots of horizontal wind direction for Episode 1 at the lidar site as (a) measured, and simulated by (b) YSU, (c) MYJ, (d) BouLac, and (e) KEPS-TPE.

the Isarco Valley with a slight delay, although KEPS-TPE shows the best agreement with observations. All schemes, except MYJ, reproduce well the structure of the valley-exit wind, the evolution of which is strictly connected with the growth of the ground-based temperature inversion. However, MYJ tends to overestimate the base of the drainage flow, reproduced at 200 m AGL.

The lidar measurements of the vertical wind component are shown in Figure 6a. The valley-exit wind is associated with positive vertical velocities at the lidar location, strengthening with the increase in the horizontal wind speed in the second part of the night and in the early morning (Figure 4a). The simulations capture the upward vertical velocity, except for MYJ, which reproduces a vertical wind speed much weaker than observations. In the MYJ simulation, the CAP is more extended towards the Isarco Valley compared with the other simulations, with a strong upward vertical velocity observed a few cells further east. This explains why the base of the valley-exit wind is reproduced at higher heights (Figures 4c and 5c). The upward motion in KEPS-TPE starts later, around 0300 LST, and again the mismatch is related to the particular

1477870x, 0, Downloaded from https://rmets.onlinelibrary.wiley.com/doi/10.1002/qj.70215 by Lorenzo Giovannini - Universita Di Trento , Wiley Online Library on [07/05/2026]. See the Terms and Conditions (https://onlinelibrary.wiley.com/terms-and-conditions) on Wiley Online Library for rules of use; OA articles are governed by the applicable Creative Commons License

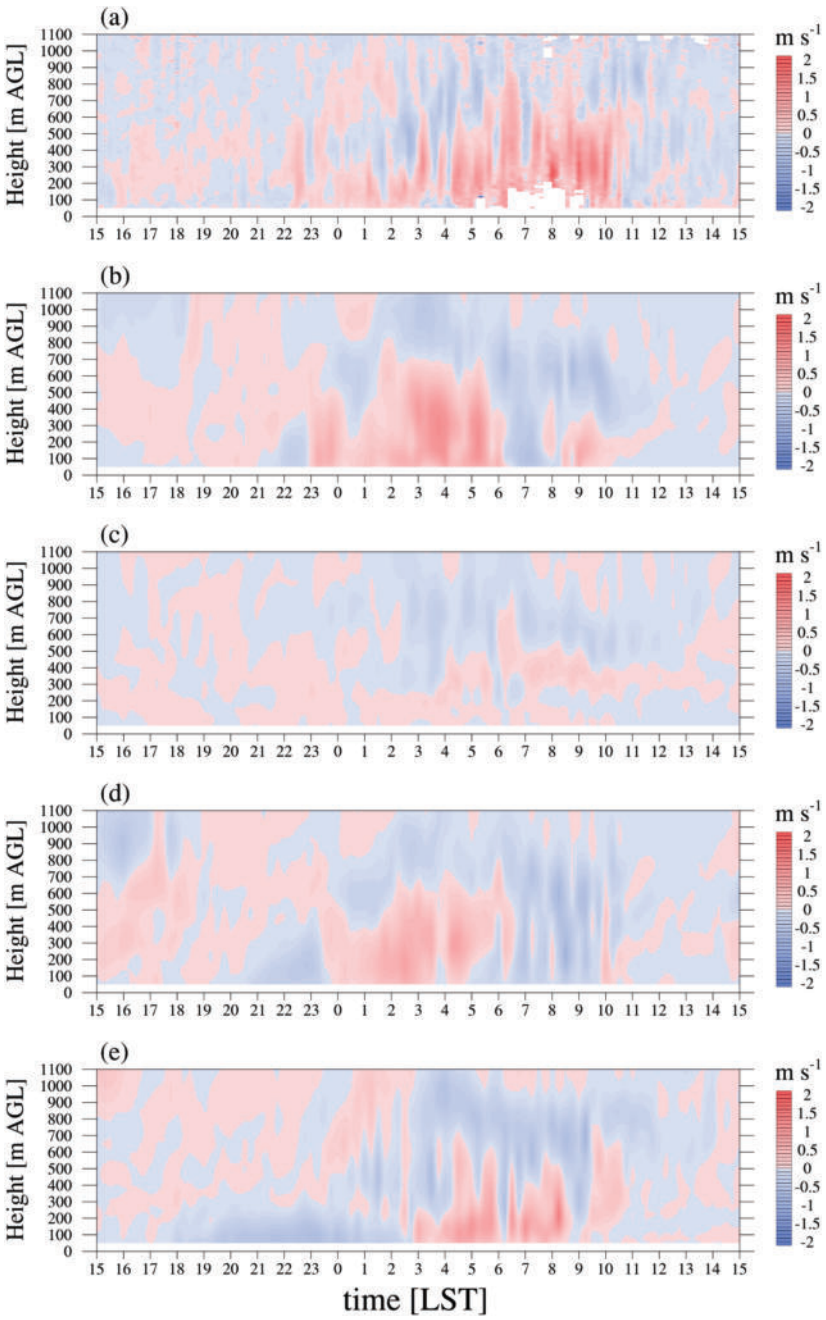


FIGURE 6 Time–height plots of vertical wind speed for Episode 1 at the lidar site as (a) measured, and simulated by (b) YSU, (c) MYJ, (d) BouLac, and (e) KEPS-TPE.

grid cell used for this analysis: a better agreement with observations would be obtained with cells immediately east of the lidar location.

4.1.1 | Quantitative evaluation of model results

For a quantitative overview of the model performance with the different PBL schemes, results and observations are compared in terms of mean error (ME) and root-mean-square error (RMSE). The atmospheric conditions at the surface are evaluated against measurements from the GWSs. ME and RMSE are estimated from hourly averages during the period January 28, 2017, 1500 LST to January 29, 2017, 1800 LST, and are summarised in Tables 1 and 2 for 2-m temperature and 10-m wind speed, respectively, with minimum ME and RMSE values at each GWS in bold.

For 2-m temperature, the ME is generally positive for all the simulations, meaning an average model overestimation, with the exception of KEPS-TPE, which shows underestimations at most GWSs. Overall, the best performance is attained by YSU, as also shown by the RMSE values and by the errors averaged over the ensemble of GWSs (<ME>, <RMSE>).

1477870x, 0, Downloaded from https://rmets.onlinelibrary.wiley.com/doi/10.1002/qj.70215 by Lorenzo Giovannini - Universita Di Trento , Wiley Online Library on [07/05/2026]. See the Terms and Conditions (https://onlinelibrary.wiley.com/terms-and-conditions) on Wiley Online Library for rules of use; OA articles are governed by the applicable Creative Commons License

TABLE 1 ME and RMSE for the 2-m temperature of the different simulations for Episode 1.

#					ME				RMSE	
T2	**GWS**	**Height (m a.s.l.)**	**YSU**	**MYJ**	**BouLac**	**KEPS-TPE**	**YSU**	**MYJ**	**BouLac**	**KEPS-TPE**
1	BR	226	**0.1**	0.6	1.4	−2.4	**1.5**	2.4	2.0	3.4
2	B0	254	**−0.2**	0.8	1.1	−2.3	**1.2**	2.3	1.8	3.1
3	GA	254	1.5	2.7	3.0	**−1.2**	**2.7**	4.1	3.9	3.3
4	ME	330	2.3	2.0	3.0	**1.0**	3.0	**2.7**	3.5	3.0
5	BC	490	2.3	2.4	3.0	**−0.8**	2.9	3.1	3.6	**1.5**
6	CA	495	**−0.1**	−0.8	0.8	−1.9	**0.9**	1.3	1.2	2.1
7	BS	585	3.1	3.3	3.9	**0.9**	3.5	3.9	4.2	**2.4**
8	FS	840	**0.3**	0.4	1.1	−0.5	**0.9**	1.4	1.2	1.4
9	SA	970	1.8	2.0	2.3	−1.8	**2.0**	2.5	2.4	2.9
10	SG	970	2.7	2.6	3.2	**2.2**	3.1	3.1	3.4	**3.0**
11	NP	1470	−0.6	−0.9	**−0.4**	−1.1	1.5	1.7	**1.4**	1.6
		<ME> <RMSE>	1.2	1.4	2.0	**−0.7**	**2.1**	2.6	2.6	2.5

Note: ME and RMSE values are computed from hourly averages of GWS measurements and WRF outputs during the interval January 28, 2017, 1500 LST to January 29, 2017, 1800 LST. <ME> and <RMSE> refer to the average values of the metrics considering all the GWSs.

TABLE 2 ME and RMSE for the 10-m wind speed of the different simulations for Episode 1.

#					ME				RMSE	
WS10	**GWS**	**Height (m a.s.l.)**	**YSU**	**MYJ**	**BouLac**	**KEPS-TPE**	**YSU**	**MYJ**	**BouLac**	**KEPS-TPE**
1	BR	226	−0.5	**0.0***	−0.3	−0.3	0.7	0.8	0.7	0.7
2	BO	254	−0.1	−0.1	**0.0***	−0.1	0.4	**0.3**	0.5	0.4
3	GA	254	0.3	**0.1**	0.3	0.2	0.6	0.6	0.6	0.6
4	ME	330	0.1	0.1	**0.0***	0.2	0.5	0.6	0.5	**0.4**
5	BC	490	2.0	0.5	1.7	**0.3**	2.3	1.2	2.0	**0.8**
6	CA	495	0.2	−0.8	0.1	−0.1	0.7	1.3	0.7	0.9
7	BS	585	0.3	−0.1	0.4	**0.0***	0.7	**0.3**	0.7	0.4
8	FS	840	−0.1	**0.0***	0.1	−0.1	0.3	0.3	0.3	0.5
9	SA	970	−0.2	−0.4	**0.0***	0.9	**0.4**	0.5	0.5	1.7
10	SG	970	0.3	**0.0***	0.2	0.2	0.6	0.4	0.4	0.6
11	NP	1470	−0.2	−0.7	−0.2	−0.4	0.6	0.9	0.6	0.7
		<ME> <RMSE>	0.2	−0.1	0.2	0.1	0.7	0.7	0.7	0.7

Note: ME and RMSE values are computed from hourly averages of GWS measurements and WRF outputs during the interval January 28, 2017, 1500 LST to January 29, 2017, 1800 LST. The symbol * means |ME| less than 0.05. <ME> and <RMSE> refer to the average values of the metrics considering all the GWSs.

Across all simulations, ME and RMSE values for 10-m wind speed are consistently low, generally remaining below 1 $m \cdot s^{-1}$ regardless of GWS location. Additionally, the spatially averaged metrics are comparable across the different simulations.

In order to understand in more detail the performance of the PBL schemes in reproducing 2-m temperature and 10-m wind speed, the time series of three GWSs, representative of the Isarco Valley (Barbiano-Colma), the Bolzano basin (Bolzano), and the Adige Valley (Bronzolo), are shown in Figure 7. All PBL schemes overestimate temperatures during night-time, except KEPS-TPE, which aligns more closely with observations. However, during daytime, KEPS-TPE tends to underestimate temperatures significantly, especially at Bolzano and Bronzolo. This suggests that the overall ME for this scheme, shown

1477870x, 0, Downloaded from https://rmets.onlinelibrary.wiley.com/doi/10.1002/qj.70215 by Lorenzo Giovannini - Universita Di Trento , Wiley Online Library on [07/05/2026]. See the Terms and Conditions (https://onlinelibrary.wiley.com/terms-and-conditions) on Wiley Online Library for rules of use; OA articles are governed by the applicable Creative Commons License

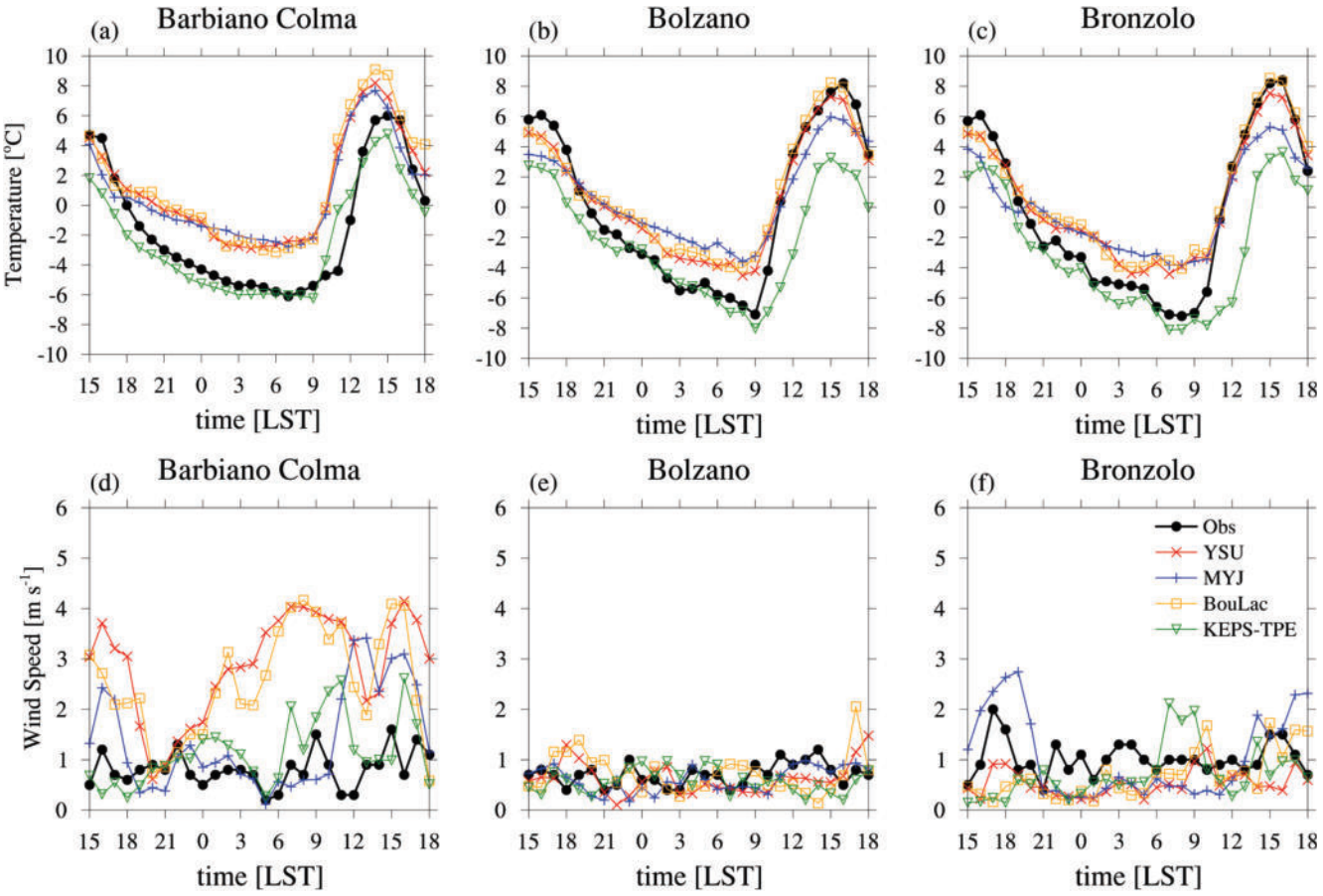


FIGURE 7 Hourly time series of 2-m temperature (upper panel) and 10-m wind speed (lower panel) at the GWSs of Barbiano-Colma, Bolzano, and Bronzolo from observations (dotted black line) and simulations for Episode 1.

in Table 1, should be attributed to daytime conditions. During daytime, temperatures are also underestimated slightly by MYJ at Bolzano and Bronzolo, whereas BouLac is close to observations. All schemes, except KEPS-TPE, tend to overestimate the near-surface temperature at Barbiano-Colma, that is, in the Isarco Valley, during daytime.

All PBL schemes reproduce a weak and mostly constant wind speed at 10-m AGL at Bolzano and Bronzolo, in agreement with observations. During night-time, YSU and BouLac overestimate wind speed at Barbiano-Colma, likely associated with the onset of the drainage flow in the Isarco Valley. Thus, these two schemes reproduce a drainage flow close to the ground, which is not confirmed by observations. Model errors at Barbiano-Colma may be due to the valley's complex geometry and narrow valley floor (about 500 m). Local atmospheric conditions, such as a ground-based temperature inversion interacting with drainage flow, may not be captured because the model's horizontal resolution does not resolve the topographic details close to the valley floor.

4.2 | February 13–14, 2017: Episode 2

Figure 8 shows the temperature time–height plots from the thermal profiler and the simulations for Episode 2. The temperature in the basin started to decrease after sunset, uniformly across all the atmospheric layers investigated. A CAP did not form in this case, due to the presence of stratocumulus clouds over the Adige Valley. During daytime, all simulations are close to observations except for MYJ, which underestimates temperature, particularly on the first day. A comparison between the surface sensible heat flux from the different simulations did not show significant differences, thus excluding the different surface-layer scheme coupled with MYJ (Section 3) as a possible cause of this underestimation (not shown). During the night, all schemes reproduce the vertical structure of the atmosphere quite well, but they mostly overestimate the cooling after sunset, especially in the evening and during the early night. This results in a temperature underestimation of 2–3°C along the whole vertical layer investigated, except for BouLac. The latter simulates

1477870x, 0, Downloaded from https://rmets.onlinelibrary.wiley.com/doi/10.1002/qj.70215 by Lorenzo Giovannini - Universita Di Trento , Wiley Online Library on [07/05/2026]. See the Terms and Conditions (https://onlinelibrary.wiley.com/terms-and-conditions) on Wiley Online Library for rules of use; OA articles are governed by the applicable Creative Commons License

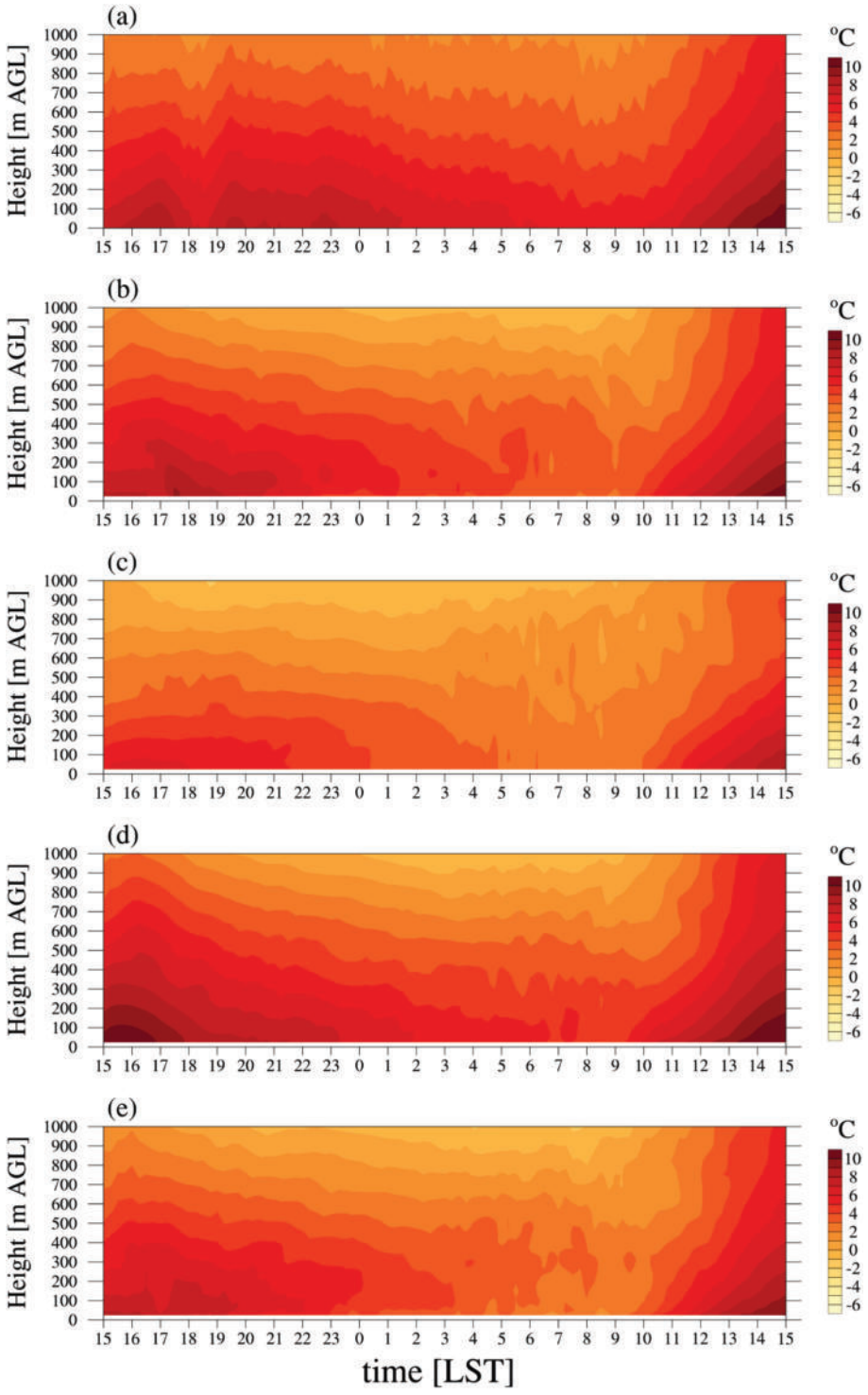


FIGURE 8 Time–height plots of temperature for Episode 2 at the temperature profiler site as (a) measured, and simulated by (b) YSU, (c) MYJ, (d) BouLac, and (e) KEPS-TPE.

a nocturnal cooling comparable with the other schemes, but, being characterised by higher temperature during daytime, it displays warmer temperatures during the night and the following morning.

The time–height plots of wind speed and direction at the lidar location from observations (Figures 9a and 10a) show a concurrent increase of the wind speed at different heights around 2200 LST, up to 600 m AGL, with a sharp change from westerly to easterly winds. The onset of the drainage flow was more uniform compared with the gradual deepening observed in Episode 1, and the increase in wind intensity was more rapid throughout the night, reaching a peak of $\sim 12\ \mathrm{m \cdot s^{-1}}$ at 0900 LST. The drainage flow died out rapidly a few hours after sunrise, around 1100 LST. All PBL schemes reproduce the onset with a delay, more significant in BouLac and YSU.

1477870x, 0, Downloaded from https://rmets.onlinelibrary.wiley.com/doi/10.1002/qj.70215 by Lorenzo Giovannini - Universita Di Trento , Wiley Online Library on [07/05/2026]. See the Terms and Conditions (https://onlinelibrary.wiley.com/terms-and-conditions) on Wiley Online Library for rules of use; OA articles are governed by the applicable Creative Commons License

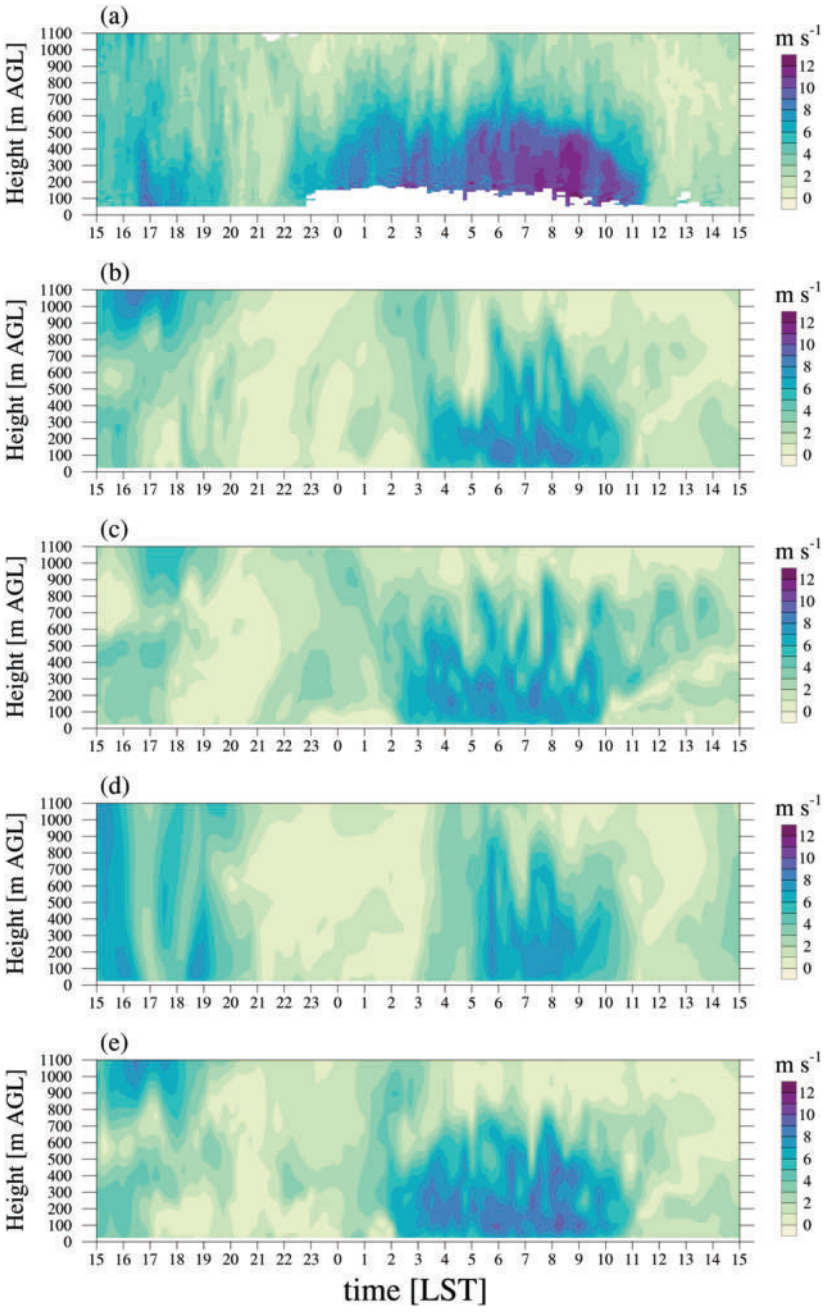


FIGURE 9 Time–height plots of horizontal wind speed for Episode 2 at the lidar site as (a) measured, and simulated by (b) YSU, (c) MYJ, (d) BouLac, and (e) KEPS-TPE.

A significant underestimation of wind speed is observed throughout the night, with KEPS-TPE being the scheme closest to observations. YSU and KEPS-TPE reproduce better the intensification of the drainage flow and the velocity peak before sunrise, the intensity and time of which are captured better by KEPS-TPE, with a maximum exactly between 0800 and 0900 LST. In the early afternoon of the first day, all schemes agree on a northwesterly wind (Figure 10), probably associated with a southerly synoptic wind channeling into the Adige Valley (a mechanism described in Whiteman & Doran, 1993) and presenting as an up-valley wind in the Isarco Valley. This channeling mechanism strengthens the up-valley wind, which is more intense in this case compared with Episode 1. This effect is simulated quite strongly by BouLac, which is also the scheme exhibiting the largest delay in the onset of the valley-exit wind, suggesting that the stronger up-valley flow impedes the development of the nocturnal local circulation.

Figure 11 shows the vertical wind speed from the lidar and the simulations. A downward flow component (negative values) was observed upon the development of the valley-exit wind. The model reproduces this feature accurately across all PBL schemes, with temporal shifts corresponding to the specific onset of the valley-exit wind in each simulation.

1477870x, 0, Downloaded from https://rmets.onlinelibrary.wiley.com/doi/10.1002/qj.70215 by Lorenzo Giovannini - Universita Di Trento , Wiley Online Library on [07/05/2026]. See the Terms and Conditions (https://onlinelibrary.wiley.com/terms-and-conditions) on Wiley Online Library for rules of use; OA articles are governed by the applicable Creative Commons License

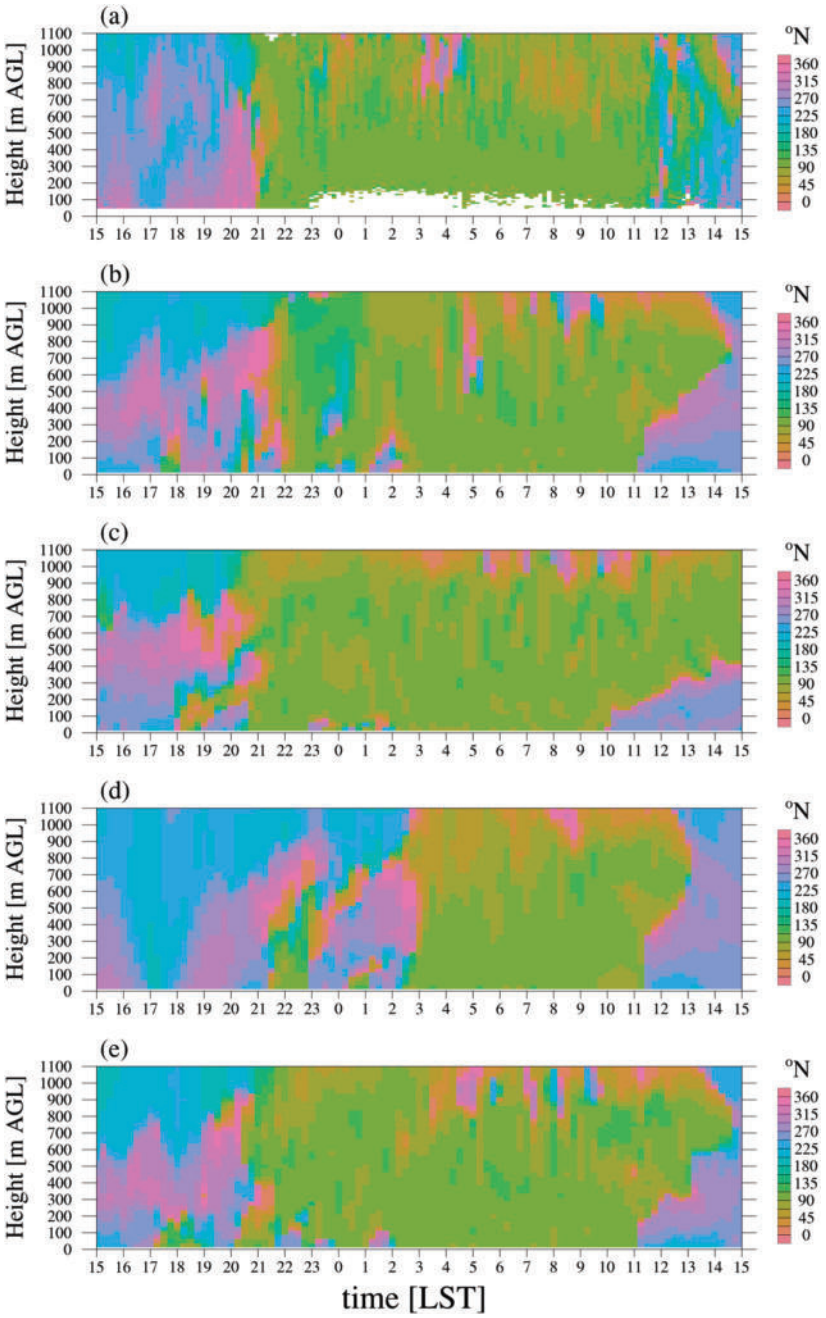


FIGURE 10 Time–height plots of horizontal wind direction for Episode 2 at the lidar site as (a) measured, and simulated by (b) YSU, (c) MYJ, (d) BouLac, and (e) KEPS-TPE.

4.2.1 | Quantitative evaluation of model results

As for Episode 1, we compare the ME and RMSE on an hourly basis, in order to evaluate the model performance quantitatively with the different PBL schemes. Results for the 11 GWSs are summarised in Tables 3 and 4 for 2-m temperature and 10-m wind speed, respectively.

A general underestimation of temperature is observed ($\sim 1°C$ for all schemes, except for MYJ with $< ME >= -2.6°C$), with BouLac having the lowest ME and RMSE across all GWSs except at Bressanone (BS). In particular, a strong underestimation is found at Bolzano (BO), which was not found in Episode 1. As mentioned in Section 2.3, Episode 2 was characterised by the presence of stratocumulus clouds over the Bolzano basin and the Adige Valley, which are likely underestimated by the model, leading to a stronger radiative cooling at the surface and a lower temperature at Bolzano. Also, for this episode, the ME of wind speed is quite small (generally less than $1\ m \cdot s^{-1}$), with little sensitivity to the PBL scheme. Considering the RMSE, MYJ shows the lowest value, although the variability between the different simulations is generally low.

Figure 12 shows the hourly time series of 2-m temperature and 10-m wind speed at the GWSs selected for Episode 1. A systematic underestimation of temperature

1477870x, 0, Downloaded from https://rmets.onlinelibrary.wiley.com/doi/10.1002/qj.70215 by Lorenzo Giovannini - Universita Di Trento , Wiley Online Library on [07/05/2026]. See the Terms and Conditions (https://onlinelibrary.wiley.com/terms-and-conditions) on Wiley Online Library for rules of use; OA articles are governed by the applicable Creative Commons License

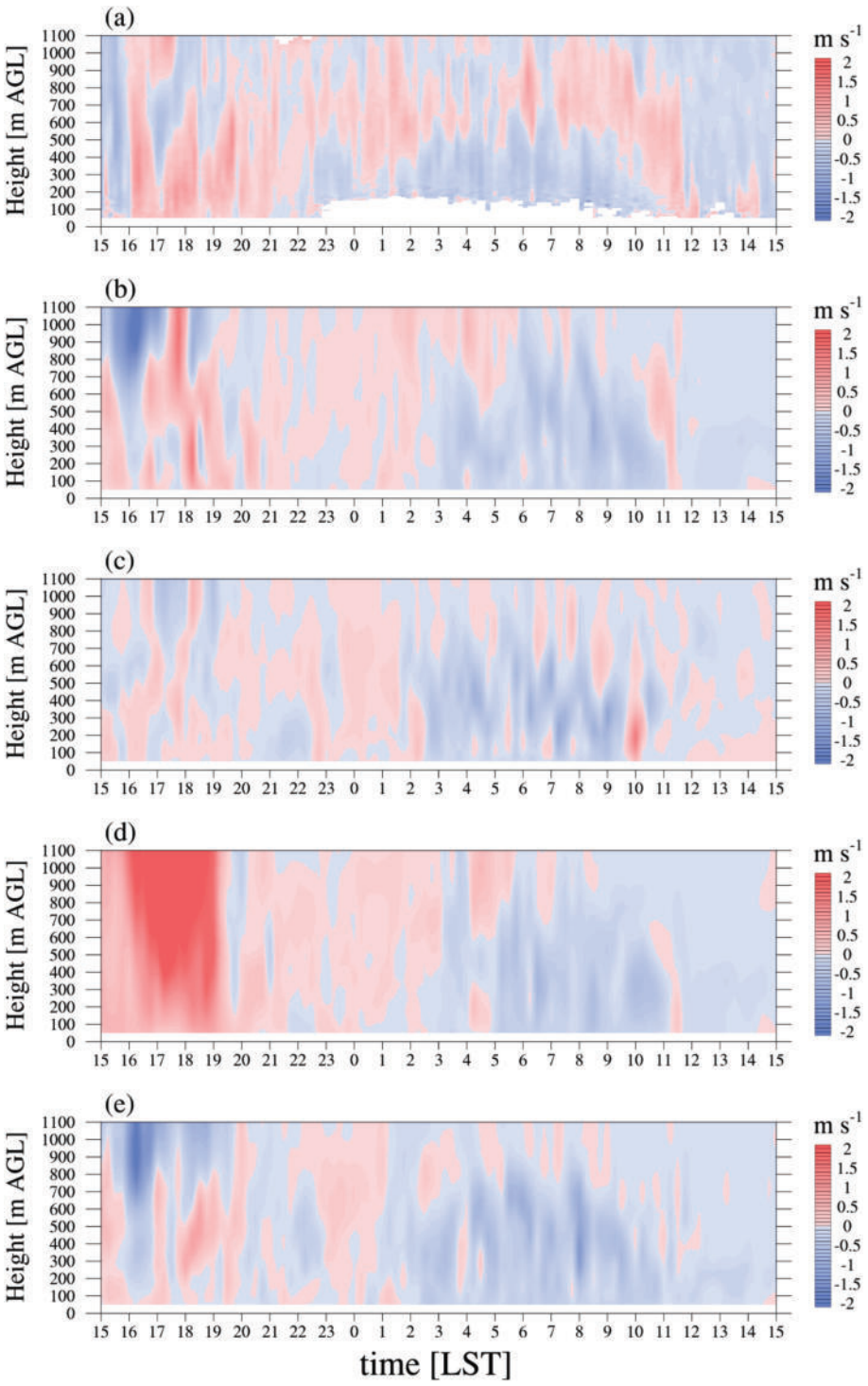


FIGURE 11 Time–height plots of vertical wind speed for Episode 2 at the lidar site as (a) measured, and simulated by (b) YSU, (c) MYJ, (d) BouLac, and (e) KEPS-TPE.

is observed for all PBL schemes, during both night-time and daytime, with BouLac being the one closest to observations. In contrast to Episode 1 (cf. Figure 7), a constant wind speed of $3\ \mathrm{m} \cdot \mathrm{s}^{-1}$ is observed at Barbiano-Colma during the night. This feature is reproduced properly by the model, and the choice of the PBL scheme mostly influences the onset and ending time of this drainage flow. At the same time, an intense wind at ground level is observed at Bolzano, which was not present in Episode 1, when a ground-based temperature inversion was well-developed in the basin. This feature is captured by YSU and KEPS-TPE, and partly by BouLac, but with a shorter duration compared with observations. Therefore, the model with the BouLac scheme underestimates the penetration of the valley-exit wind at low levels in the Bolzano basin, possibly due to the overestimation of the temperature stratification (cf. Figure 8d). On the other hand, MYJ is completely missing the nocturnal wind

1477870x, 0, Downloaded from https://rmets.onlinelibrary.wiley.com/doi/10.1002/qj.70215 by Lorenzo Giovannini - Universita Di Trento , Wiley Online Library on [07/05/2026]. See the Terms and Conditions (https://onlinelibrary.wiley.com/terms-and-conditions) on Wiley Online Library for rules of use; OA articles are governed by the applicable Creative Commons License

TABLE 3 ME and RMSE for the 2-m temperature of the different simulations for Episode 2.

#					ME				RMSE	
T2	**GWS**	**Height (m a.s.l.)**	**YSU**	**MYJ**	**BouLac**	**KEPS-TPE**	**YSU**	**MYJ**	**BouLac**	**KEPS-TPE**
1	BR	226	−2.4	−3.8	**−1.1**	−3.0	2.6	3.8	**1.3**	3.2
2	BO	254	−2.7	−4.0	**−1.2**	−3.1	3.0	4.2	**1.4**	3.5
3	GA	290	−1.9	−2.6	**−0.4**	−2.4	2.2	2.8	**1.3**	2.7
4	ME	330	−1.5	−2.7	**−0.8**	−2.0	1.9	3.0	**1.3**	2.3
5	BC	490	−1.0	−3.0	**−0.1**	−1.6	1.6	3.4	**1.1**	2.1
6	CA	495	−1.5	−3.1	**−0.9**	−2.0	1.8	3.3	**1.1**	2.2
7	BS	585	0.4	−1.3	1.4	**−0.3**	**1.1**	2.0	1.6	1.2
8	FS	840	−0.9	−2.2	**−0.2**	−1.4	1.1	2.3	**0.6**	1.5
9	SA	970	−1.2	−2.2	**−0.7**	−1.4	1.8	2.5	**1.5**	2.0
10	SG	970	−1.0	−2.0	**−0.6**	−1.2	1.4	2.2	**1.2**	1.6
11	NP	1470	−0.5	−2.0	**0.3**	−0.8	1.7	2.3	**1.6**	2.0
		<ME> <RMSE>	−1.3	−2.6	**−0.4**	−1.8	1.8	2.9	**1.3**	2.2

Note: ME and RMSE values are computed from hourly averages of GWS measurements and WRF outputs during the interval February 13, 2017, 1500 LST to February 14, 2017, 1800 LST. <ME> and <RMSE> refer to the average values of the metrics considering all the GWSs.

TABLE 4 ME and RMSE for the 10-m wind speed of the different simulations for Episode 2.

#					ME				RMSE	
WS10	**GWS**	**Height (m a.s.l.)**	**YSU**	**MYJ**	**BouLac**	**KEPS-TPE**	**YSU**	**MYJ**	**BouLac**	**KEPS-TPE**
1	BR	226	−0.7	−0.7	**0.4**	−0.9	1.5	1.7	**1.0**	1.7
2	BO	254	−1.0	−1.6	**−0.8**	−1.0	2.1	2.3	2.0	**1.8**
3	GA	290	0.4	0.4	0.4	**0.3**	0.7	0.7	0.9	0.7
4	ME	330	0.5	0.4	**0.3**	0.4	1.3	**0.7**	1.2	1.2
5	BC	490	1.0	**0.2**	1.2	1.1	1.9	**1.0**	2.3	1.6
6	CA	495	−0.6	−0.6	**−0.1**	−0.4	1.2	1.2	**1.0**	1.2
7	BS	585	**−0.1**	−0.6	0.6	−0.2	1.3	1.2	1.3	**1.0**
8	FS	840	**0.0***	−0.2	0.1	0.1	0.6	**0.5**	0.8	0.7
9	SA	970	−0.1	−0.5	0.1	−0.3	**0.9**	1.0	1.1	1.1
10	SG	970	0.4	**0.1**	0.5	0.4	0.7	**0.4**	0.8	0.7
11	NP	1470	0.2	0.1	0.2	0.1	0.8	0.8	1.0	0.8
		<ME> <RMSE>	0.0*	−0.3	0.3	−0.0*	1.2	**1.0**	1.2	1.1

Note: ME and RMSE values are computed from hourly averages of GWS measurements and WRF outputs during the interval February 13, 2017, 1500 LST to February 14, 2017, 1800 LST. The symbol * means |ME| or RMSE less than 0.05. <ME> and <RMSE> refer to the average values of the metrics considering all the GWSs.

increase at Bolzano GWS, even if the wind speed and direction are captured at the lidar location (Figures 9c and 10c).

At Bronzolo, the wind speed is very weak during night-time, supporting the suggestion that the wind observed at Bolzano is related to the drainage flow of the Isarco Valley. A peak in wind speed is observed during the afternoon, related to the strong up-valley flow of the Adige Valley and reproduced only by the BouLac scheme. This corroborates the hypothesis drawn from observations that a channeling mechanism was strengthening the up-valley flow in the Adige Valley. However, the comparison at Barbiano-Colma shows that all schemes, except MYJ, overestimate this effect in the Isarco Valley. This can explain

1477870x, 0, Downloaded from https://rmets.onlinelibrary.wiley.com/doi/10.1002/qj.70215 by Lorenzo Giovannini - Universita Di Trento , Wiley Online Library on [07/05/2026]. See the Terms and Conditions (https://onlinelibrary.wiley.com/terms-and-conditions) on Wiley Online Library for rules of use; OA articles are governed by the applicable Creative Commons License

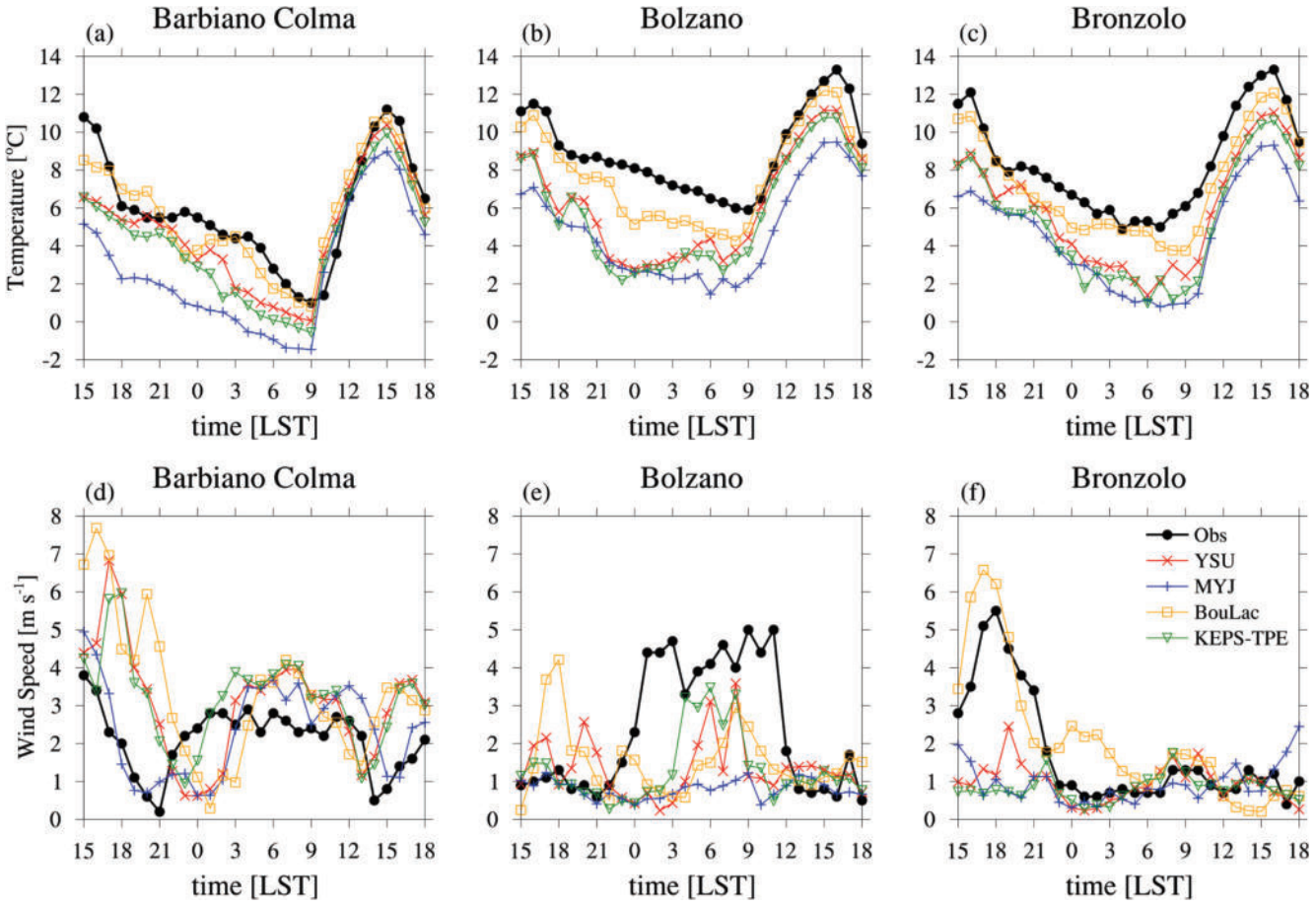


FIGURE 12 Hourly time series of 2-m temperature (upper panel) and 10-m wind speed (lower panel) at the GWSs of Barbiano-Colma, Bolzano, and Bronzolo from observations (dotted black line) and simulations for Episode 2.

the delay, compared with lidar observations, in the onset of the valley-exit wind, observed in all simulations (Figure 9).

5 | SPATIAL CHARACTERISTICS OF THE VALLEY-EXIT WIND AND INTERACTION WITH THE CAP

Numerical simulations provide a means to analyse the spatial characteristics of the valley-exit flow and the mechanisms governing its interaction with the Bolzano basin air, complementing the information from sparse point measurements. For this purpose, the YSU scheme was selected for Episode 1 and the KEPS-TPE scheme for Episode 2. These specific simulations were chosen due to their good agreement with the lidar observations regarding both horizontal (Figures 4 and 9) and vertical (Figures 6 and 11) wind velocity components. However, as the verification analysis revealed that no single scheme clearly outperforms the others, the findings presented in this section remain robust regardless of the specific simulation selected.

5.1 | Episode 1: Interaction with the CAP

For Episode 1, Figure 13 presents horizontal cross-sections of the wind field at different hours of the night at ~700 m a.s.l. (top row) and 10 m AGL (bottom row). At ~700 m a.s.l., the down-valley flow is visible both in the Adige Valley and in the Isarco Valley (Figure 13a). The modeled flow in the Isarco Valley shows that larger wind speeds are reached in the lower section of the valley, corroborating the hypothesis drawn from the observations that the nocturnal drainage current presents valley-exit jet characteristics. As night progresses, at 700 m a.s.l. the valley-exit flow intensifies and, once entering the basin, it veers southward before spreading horizontally in the Adige Valley (Figure 13b,c). It veers southward before reaching the mountains in the westward direction, which may point to a peculiar effect of the valley geometry or to an interaction with the down-valley flow of the Adige Valley. Just beyond the valley exit, the 10-m wind speed decreases abruptly (Figure 13e,f). This suggests that a well-developed CAP covers the basin at low levels and the drainage flow is not able to split, for example, flowing partly above and

1477870x, 0, Downloaded from https://rmets.onlinelibrary.wiley.com/doi/10.1002/qj.70215 by Lorenzo Giovannini - Universita Di Trento , Wiley Online Library on [07/05/2026]. See the Terms and Conditions (https://onlinelibrary.wiley.com/terms-and-conditions) on Wiley Online Library for rules of use; OA articles are governed by the applicable Creative Commons License

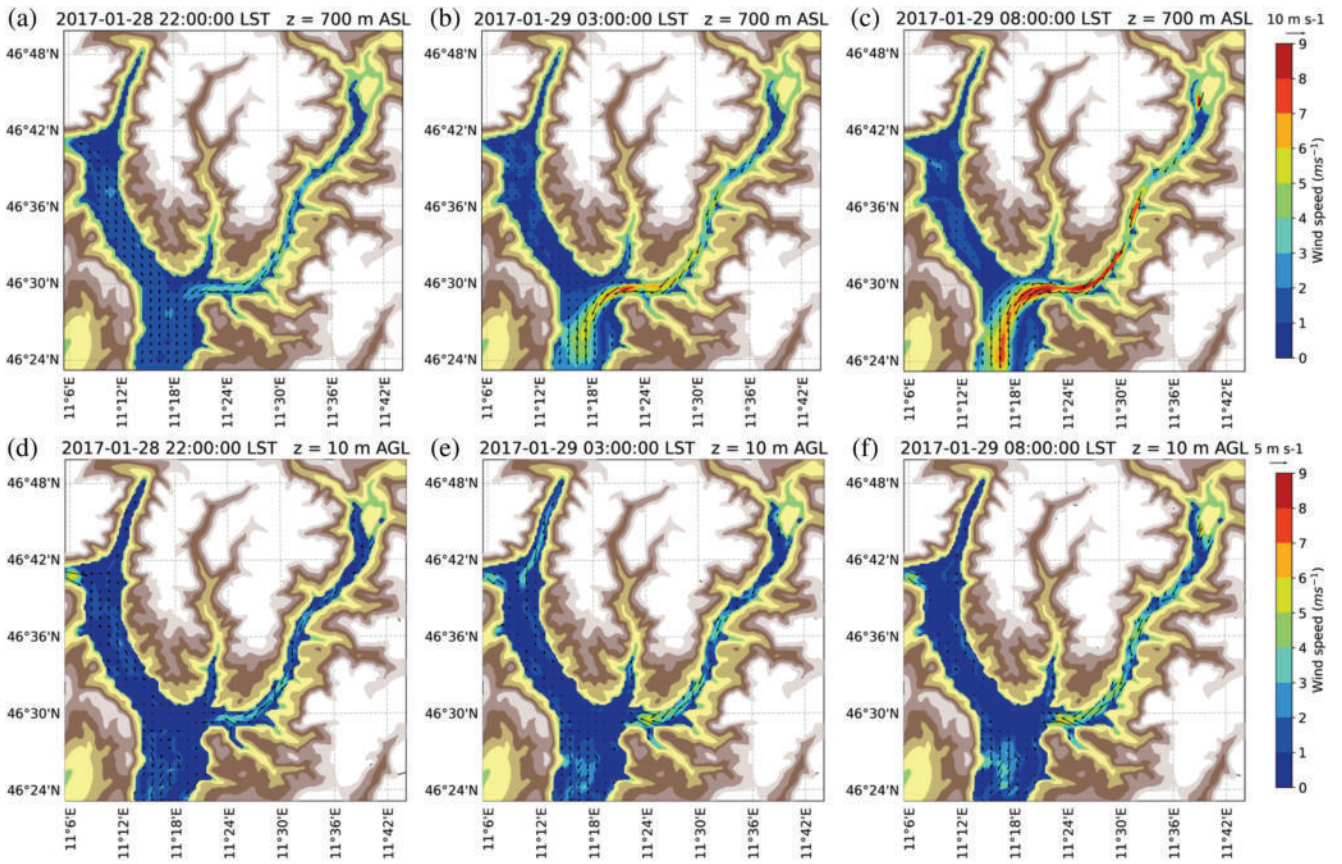


FIGURE 13 Horizontal cross-sections of hourly wind speed at (a–c) 700 m a.s.l. and (d–f) 10 m AGL for Episode 1, as reproduced by the YSU simulation at (a,d) 2200 LST on January 28, 2017, (b,e) 0300 LST on January 29, 2017, and (c,f) 0800 LST on January 29, 2017.

partly below the CAP, as observed in Cuxart *et al.* (2007), or flowing around it. The CAP blocks the valley-exit flow from penetrating at low levels and the entire drainage flow is forced to lift over the colder, denser air within the basin.

Figure 14 shows vertical cross-sections along the Isarco Valley displaying the horizontal wind speed parallel to the section (Figure 14b,e), potential temperature (Figure 14c,f), and vertical wind speed (Figure 14d,g) along the black line shown in Figure 14a. This transect was chosen to follow the topography along the main axis of the Isarco Valley and to capture the transition to the Bolzano basin. In the first hours of the night, the down-valley flow (corresponding to negative values in Figure 14b) is weak, shallow, and uniformly developed. Throughout the night, its depth increases across the whole Isarco Valley, with stronger speeds at the exit region (Figure 14e). Here, the flow sinks and compresses, confirming that its intensification is due to mechanisms similar to those leading to the formation of valley-exit winds. The sharp flow deceleration at the exit region extends across multiple vertical layers and the isentropic lines show that it is connected to the depth of the CAP in the basin. The cross-sections of potential temperature (Figure 14c,f) show that a CAP is already present at the beginning of the night, covering the whole basin. Conversely, the Isarco Valley cools uniformly but maintains a higher potential temperature than the basin. In the morning, a strong CAP still persists, with a sharp boundary at the valley exit. Consistent with lidar observations (Figure 11a), the model reproduces upward velocities from the surface up to ~ 800 m a.s.l. at the valley exit (Figure 14g). This suggests that the CAP is acting as a downstream block to the flow (Reeves & Lin, 2006).

Downward velocities just above the rising layer are simulated, suggesting that the valley-exit wind rises above the CAP while it is still sinking and compressing, which may contribute to intensifying the flow further.

5.2 | Episode 2

For Episode 2, the horizontal wind field at ~ 700 m a.s.l., shown in Figure 15a–c, exhibits a pattern similar to Episode 1 (cf. Figure 13a–c). However, the flow tends to be weaker and spreads more broadly across the Adige

1477870x, 0, Downloaded from https://rmets.onlinelibrary.wiley.com/doi/10.1002/qj.70215 by Lorenzo Giovannini - Universita Di Trento , Wiley Online Library on [07/05/2026]. See the Terms and Conditions (https://onlinelibrary.wiley.com/terms-and-conditions) on Wiley Online Library for rules of use; OA articles are governed by the applicable Creative Commons License

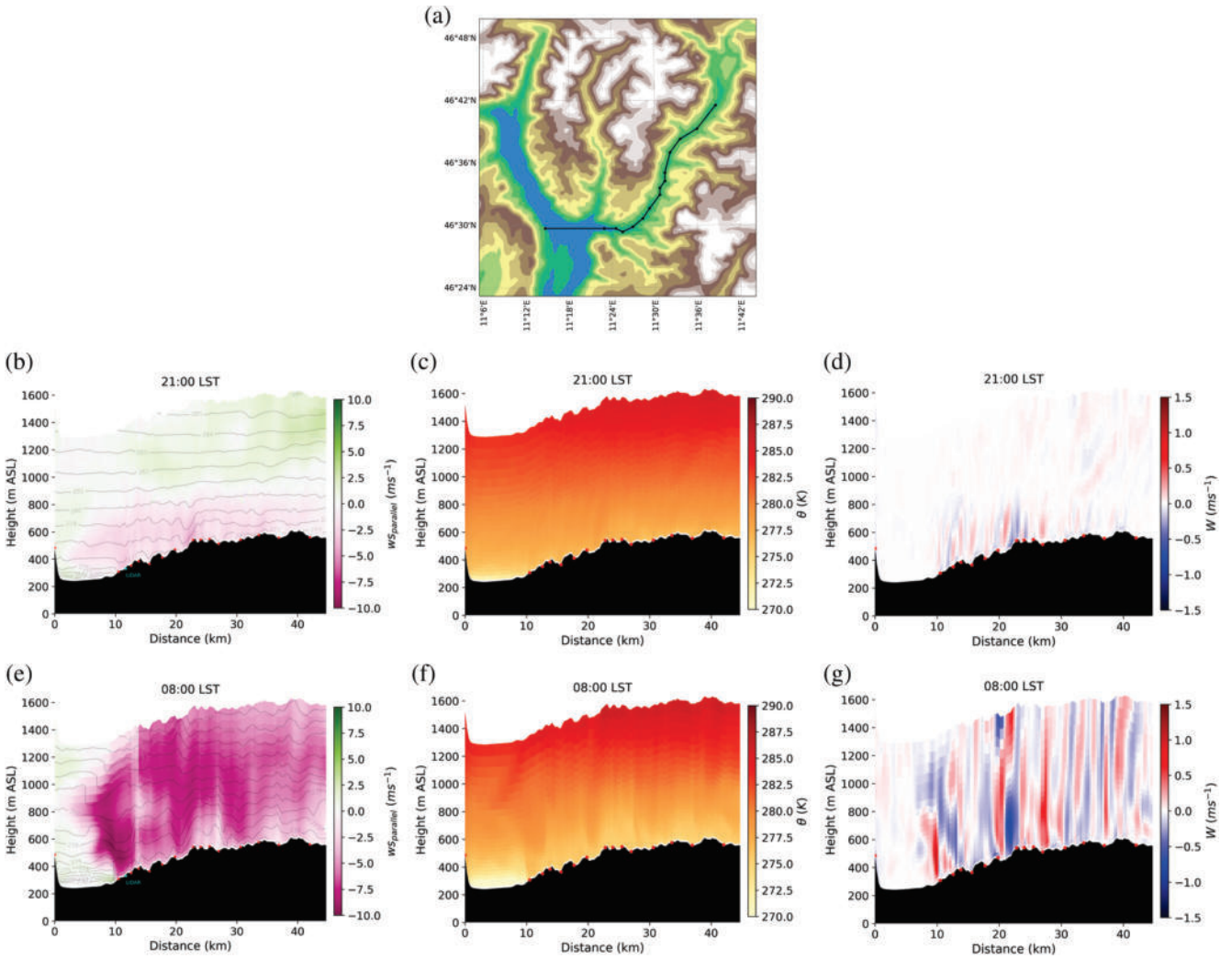


FIGURE 14 Vertical cross-sections from the YSU simulation along the Isarco Valley, following the black line in panel (a), for Episode 1 at (b–d) 2100 LST on January 28, 2017 and (e–g) 0800 LST on January 29, 2017. Panels (b) and (e) show the wind speed parallel to the cross-section plane (color scale), with negative values for easterly (down-valley) flow, and the potential temperature (gray lines), panels (c) and (f) show the potential temperature, and panels (d) and (g) show the vertical wind speed. The terrain height is shown in black, with the red points as delimiters between the different cross-sections (see panel a).

Valley, which is likely a consequence of its weaker intensity. Near the surface, wind speeds similar to Episode 1 are reproduced by the model at the valley exit, but in this case the down-valley flow propagates further into the basin. This spatial structure of the flow is consistent with the observations from the Bolzano GWS, which measured near-surface winds of about 4 $m \cdot s^{-1}$ for Episode 2 (Figure 12), in contrast with the calm conditions for Episode 1 (Figure 7). Vertical-cross-sections analogous to Figure 14 are shown in Figure 16. The onset of the down-valley flow in the Isarco Valley occurs later than in Episode 1, a delay attributed to the southerly synoptic wind channeling mentioned in Section 4.2. The atmosphere is less stratified, as evidenced by the wider spacing of the isotherms in Figure 16a,d compared with Episode 1 (Figure 14a,d). By early morning, the down-valley flow has reached depths similar to Episode 1 and again it sinks and compresses at the exit, confirming the hydraulic flow transition as the main dynamical mechanism for flow intensification. However, in this case the flow is able to penetrate into the Bolzano basin down to the lowest layers, because the valley-exit wind has a lower potential temperature than the air in the basin (Figure 16e). Accordingly, the exit region is characterised by a downward motion even at the ground (Figure 16f), with the flow following the topography toward the basin.

6 | CONCLUSIONS

An intense field campaign took place in a mountain basin in the Adige Valley (Italian Alps) during winter 2017,

1477870x, 0, Downloaded from https://rmets.onlinelibrary.wiley.com/doi/10.1002/qj.70215 by Lorenzo Giovannini - Universita Di Trento , Wiley Online Library on [07/05/2026]. See the Terms and Conditions (https://onlinelibrary.wiley.com/terms-and-conditions) on Wiley Online Library for rules of use; OA articles are governed by the applicable Creative Commons License

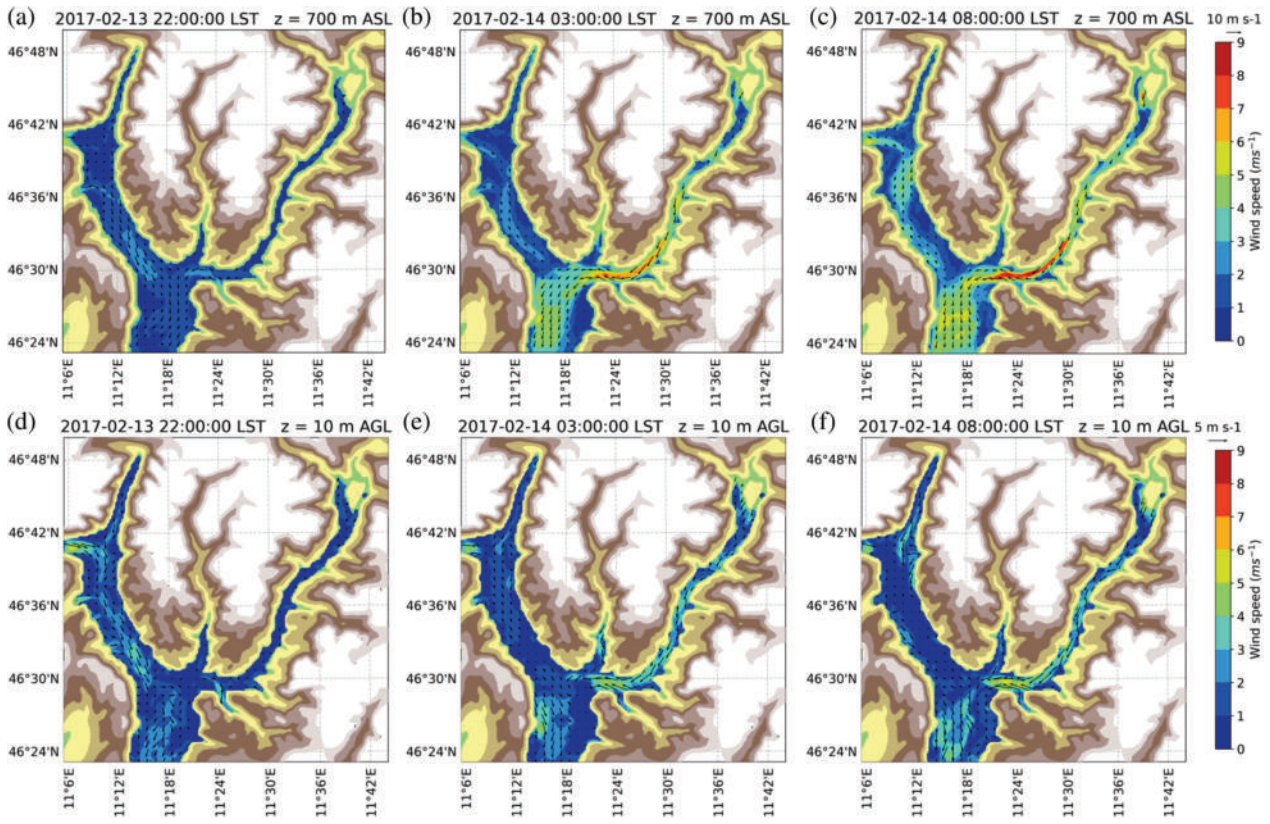


FIGURE 15 Horizontal cross-sections of hourly wind speed at (a–c) 700 m a.s.l. and (d–f) 10 m AGL for Episode 2, as reproduced by the KEPS-TPE simulation at (a,d) 2200 LST on February 13 2017, (b,e) 0300 LST on February 14, 2017, and (c,f) 0800 LST on February 14, 2017.

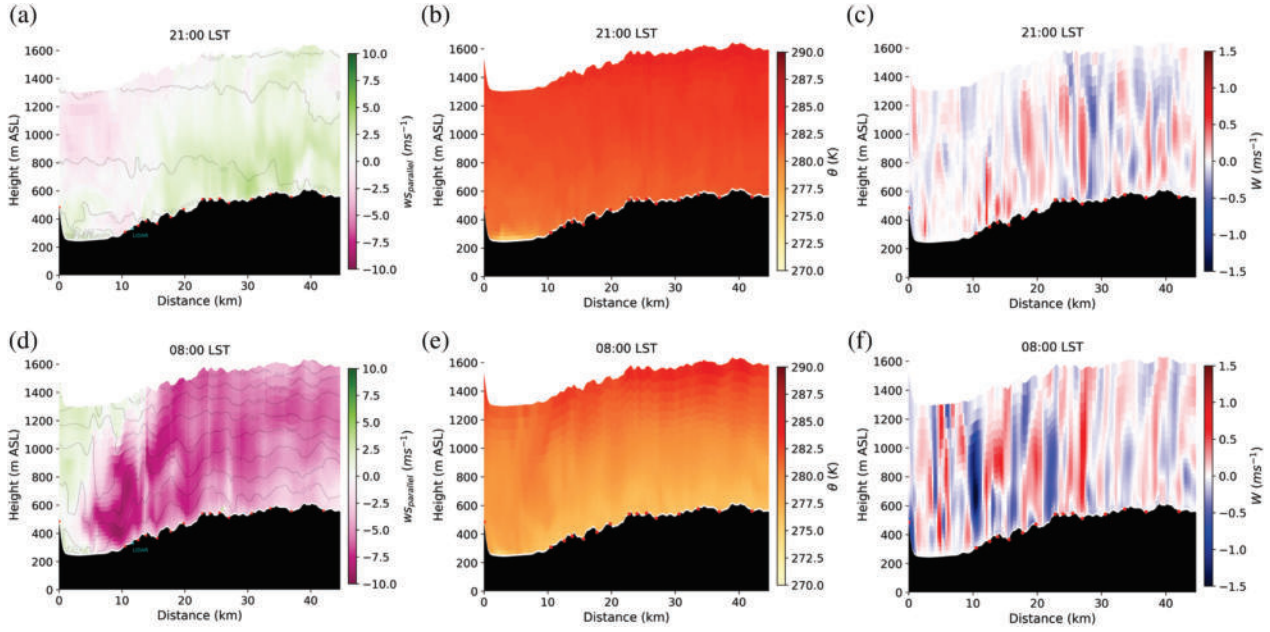


FIGURE 16 Vertical cross-sections from the KEPS-TPE simulation along the Isarco Valley, following the black line in Figure 14a, for Episode 2 at (a–c) 2100 LST on February 13, 2017 and (d–f) 0800 LST on February 14, 2017. Panels (a) and (d) show the wind speed parallel to the cross-section plane (negative values indicate down-valley flow), together with potential temperature contours (gray). Panels (b) and (e) show the wind speed parallel to the cross-section plane (color scale) with potential temperature (gray contours). Panels (c) and (f) show potential temperature. The terrain height is shown in black; red points delimit the different cross-sections (see Figure 14a).

1477870x, 0, Downloaded from https://rmets.onlinelibrary.wiley.com/doi/10.1002/qj.70215 by Lorenzo Giovannini - Universita Di Trento , Wiley Online Library on [07/05/2026]. See the Terms and Conditions (https://onlinelibrary.wiley.com/terms-and-conditions) on Wiley Online Library for rules of use; OA articles are governed by the applicable Creative Commons License

including surface measurements and vertical profiles of temperature and wind speed and direction. Wind-profile measurements were performed near the exit of a tributary valley into the basin, and strong wind speeds around 10 $m \cdot s^{-1}$ were observed at night, with maximum intensity close to sunrise, pointing to a strong drainage flow from the tributary valley. Similar speeds in mountainous environments have been observed in regions where topography changes abruptly (e.g., canyon and valley exits) and were attributed to the sinking and compression of a cold-air flow in those regions, with a consequent acceleration of the flow. These flows are commonly named valley-exit jet/flows and the present study aimed to investigate the characteristics of the drainage current into the basin and understand whether the flow behaves as a valley-exit flow. Combining the information from wind and temperature measurements, observations also showed that the thermal stratification in the basin influences the flow once it reaches the basin. This feature was investigated in the present study by comparing the nocturnal circulation in two different wintertime cases: one with a strong ground-based temperature inversion, which led to the development of a CAP during night-time, and one without.

The sparse information from point measurements was complemented with high-resolution ($\Delta \sim 300$ m) numerical simulations, performed with the WRF model. Model results are used to understand the main mechanism for the flow intensification at the valley exit, as well as the interaction of the flow with the CAP. Due to the challenges of numerical models in representing the very stable boundary layer, the choice of the PBL scheme may play a significant role in the correct representation of this nocturnal circulation. Thus, a comparison of simulations with different PBL schemes was performed to assess their possible impact on the model results and ensure robustness of the conclusions. Four PBL schemes (YSU, MYJ, BouLac, KEPS-TPE) have been tested and compared with measurements from a temperature profiler, a Doppler wind lidar, and 2-m temperature and 10-m wind speed from several ground weather stations on the valley floor and sidewalls.

Simulation results indicate that the model is able to capture the main structure of the wind flow at the lidar location, quite independently of the PBL scheme, whereas the thermal structure at the thermal profiler location is more sensitive to the specific scheme. When a strong CAP develops during night-time, the thermal stratification is captured best by a PBL parameterisation including, among other things, a prognostic equation for temperature variance and a counter-gradient term (KEPS-TPE: Zonato *et al.*, 2022).

Cross-sections of the wind field from the simulations confirm that the drainage flow has valley-exit wind characteristics: it sinks and compresses when approaching the exit of the valley with an increase in the wind speed. Cross-sections of potential temperature also suggest that the CAP covers the entire basin, such that the valley-exit wind rises as it encounters the cold air inside the basin, instead of splitting above and below the CAP or flowing around it.

When the thermal stratification in the basin is weaker, all PBL schemes capture the vertical structure of the lower atmospheric layers, with an overall underestimation of temperature by 2–3 °C. This was likely caused by an inadequate representation of the stratocumulus clouds over the Adige Valley that were present in this case. All simulations produce a delay in the onset of the valley-exit wind, which was attributed to a strong up-valley wind in the afternoon lasting until the evening. Observations suggest a channeling mechanism, induced by the synoptic flow, in the Adige Valley, but the model also tends to reproduce and strengthen this effect in the Isarco Valley.

During the night, a downward motion at the lidar location and strong 10-m wind speed at the GWSs along the path of the valley-exit wind are observed. This suggests that, with a weaker thermal stratification, the flow is able to reach the low layers in the basin, as also supported by cross-sections of wind speed from the numerical simulations.

This work provides a broad picture of a peculiar phenomenon of the local circulation in the Adige Valley. However, analogous situations may be found in other regions. Similar flows are reported at the exit of narrow valleys into wider adjacent areas (Jiménez *et al.*, 2019; Pfister *et al.*, 2024; Zängl, 2004), and drainage-flow interactions with cold air inside a main valley (Muñoz *et al.*, 2020; Neff & King, 1987, 1989; Pinto *et al.*, 2006) are observed in different locations worldwide. Thus, results from this work may be useful to interpret the mechanisms and factors controlling similar circulations at other locations.

Future investigations aim at understanding better the impact of the valley-exit flow on turbulent vertical mixing over the area. Lampert *et al.* (2016) suggests that the occurrence of a nocturnal low-level jet influences the anisotropic characteristics of turbulence in the stable boundary layer, by enhancing the damping of the vertical wind variance with respect to horizontal wind variances (on scales of a few hundred meters), and it would be interesting to investigate whether these flows can drive turbulence towards a particular state of anisotropy of the Reynolds stress tensor, as observed for waves in a stable stratified atmosphere (Gucci *et al.*, 2023). Comparison of cases with and without the arrival of the valley-exit flow in the basin could be used for this purpose. However, a new ad hoc field campaign including turbulence measurements would be required.

1477870x, 0, Downloaded from https://rmets.onlinelibrary.wiley.com/doi/10.1002/qj.70215 by Lorenzo Giovannini - Universita Di Trento , Wiley Online Library on [07/05/2026]. See the Terms and Conditions (https://onlinelibrary.wiley.com/terms-and-conditions) on Wiley Online Library for rules of use; OA articles are governed by the applicable Creative Commons License

ACKNOWLEDGMENT

The authors thank two anonymous reviewers who carefully revised the article and provided us with helpful comments, which improved the work substantially. The authors acknowledge Eco-Center s.p.a. for financial support to the project, in particular for renting the Doppler wind lidar. The Weather Service of the Autonomous Province of Bolzano provided data from its weather stations. The Environmental Agency of the Autonomous Province of Bolzano provided data from the microwave temperature profiler. Open access publishing facilitated by Università degli Studi di Trento, as part of the Wiley - CRUI-CARE agreement.

CONFLICT OF INTEREST STATEMENT

The authors declare no conflict of interest.

DATA AVAILABILITY STATEMENT

The data that support the findings of this study are available from the corresponding authors upon request.

ENDNOTES

[1]https://worldview.earthdata.nasa.gov.
[2]http://www.viewfinderpanoramas.org.
[3]http://www.eea.europa.eu.

ORCID

Federica Gucci https://orcid.org/0000-0003-3583-9765
Dino Zardi https://orcid.org/0000-0002-3573-3920
Lorenzo Giovannini https://orcid.org/0000-0003-1650-0344

REFERENCES

Adler, B., Gohm, A., Kalthoff, N., Babić, N., Corsmeier, U., Lehner, M. et al. (2021) CROSSINN: a field experiment to study the three-dimensional flow structure in the Inn Valley, Austria. *Bulletin of the American Meteorological Society*, 102, E38–E60. Available from: https://doi.org/10.1175/BAMS-D-19-0283.1

Adler, B., Wilczak, J.M., Kenyon, J., Bianco, L., Djalalova, I.V., Olson, J.B. et al. (2023) Evaluation of a cloudy cold-air pool in the Columbia River basin in different versions of the High-Resolution Rapid Refresh (HRRR) model. *Geoscientific Model Development*, 16, 597–619. Available from: https://doi.org/10.5194/gmd-16-597-2023

Arduini, G., Staquet, C. & Chemel, C. (2016) Interactions between the nighttime valley-wind system and a developing cold-air pool. *Boundary-Layer Meteorology*, 161, 49–72. Available from: https://doi.org/10.1007/s10546-016-0155-8

Arthur, R.S., Lundquist, K.A. & Olson, J.B. (2021) Improved prediction of cold-air pools in the weather research and forecasting model using a truly horizontal diffusion scheme for potential temperature. *Monthly Weather Review*, 149, 155–171. Available from: https://doi.org/10.1175/MWR-D-20-0234.1

Babić, N., Adler, B., Gohm, A., Kalthoff, N., Haid, M., Lehner, M. et al. (2021) Cross-valley vortices in the Inn valley, Austria: structure, evolution and governing force imbalances. *Quarterly Journal of the Royal Meteorological Society*, 147, 3835–3861. Available from: https://doi.org/10.1002/qj.4159

Banta, R.M. & Gannon, P.T. (1995) Influence of soil moisture on simulations of katabatic flow. *Theoretical and Applied Climatology*, 52, 85–94. Available from: https://doi.org/10.1007/BF00865509

Banta, R.M., Mahrt, L., Vickers, D., Sun, J., Balsley, B.B., Pichugina, Y.L. et al. (2007) The very stable boundary layer on nights with weak low-level jets. *Journal of the Atmospheric Sciences*, 64, 3068–3090. Available from: https://doi.org/10.1175/JAS4002.1

Banta, R.M., Olivier, L.D., Gudiksen, P.H. & Lange, R. (1996) Implications of small-scale flow features to modeling dispersion over complex terrain. *Journal of Applied Meteorology and Climatology*, 35, 330–342. Available from: https://doi.org/10.1175/1520-0450(1996)035<0330:IOSSFF>2.0.CO;2

Banta, R.M., Olivier, L.D., Neff, W.D., Levinson, D.H. & Ruffieux, D. (1995) Theoretical and applied climatology influence of canyon-induced flows on flow and dispersion over adjacent plains. *Theoretical and Applied Climatology*, 52, 27–42. Available from: https://doi.org/10.1007/BF00865505

Bisignano, A., Carotenuto, F., Zaldei, A. & Giovannini, L. (2022) Field calibration of a low-cost sensors network to assess traffic-related air pollution along the Brenner highway. *Atmospheric Environment*, 275, 119008. Available from: https://doi.org/10.1016/j.atmosenv.2022.119008

Bougeault, P. & Lacarrére, P. (1989) Parameterization of orography-induced turbulence in a mesobeta scale model. *Monthly Weather Review*, 117, 1872–1890. Available from: https://doi.org/10.1175/1520-0493(1989)117<1872:POOITI>2.0.CO;2

Boyko, V. & Vercauteren, N. (2024) Simulating the unsteady stable boundary layer with a stochastic stability equation. *Journal of Geophysical Research: Atmospheres*, 129, e2023JD039370. Available from: https://doi.org/10.1029/2023JD039370

Chow, K.F., Weigel, A.P., Street, R.L., Rotach, M.W. & Xue, M. (2006) High-resolution large-eddy simulations of flow in a steep alpine valley. Part I: methodology, verification, and sensitivity experiments. *Journal of Applied Meteorology and Climatology*, 45, 63–86. Available from: https://doi.org/10.1175/JAM2322.1

Chrust, M.F., Whiteman, C.D. & Hoch, S.W. (2013) Observations of thermally driven wind jets at the exit of Weber Canyon, Utah. *Journal of Applied Meteorology and Climatology*, 52, 1187–1200. Available from: https://doi.org/10.1175/JAMC-D-12-0221.1

Clements, C.B., Whiteman, C.D. & Horel, J.D. (2003) Cold-air-pool structure and evolution in a mountain basin: Peter Sinks, Utah. *Journal of Applied Meteorology*, 42, 752–768. Available from: https://doi.org/10.1175/1520-0450(2003)042<0752:CSAEIA>2.0.CO;2

Cuxart, J.R., Jiménez, M.A. & Martínez, D. (2007) Nocturnal meso-beta basin and katabatic flows on a midlatitude island. *Monthly Weather Review*, 135, 918–932. Available from: https://doi.org/10.1175/MWR3329.1

Daly, C., Conklin, D. & Unsworth, M. (2009) Local atmospheric coupling in complex topography alters climate change impacts. *International Journal of Climatology*, 30, 1857–1864. Available from: https://doi.org/10.1002/joc.2007

De Wekker, S.F.J. & Whiteman, C.D. (2006) On the time scale of nocturnal boundary layer cooling in valleys and basins and over plains. *Journal of Applied Meteorology and Climatology*, 45, 813–820. Available from: https://doi.org/10.1175/JAM2378.1

1477870x, 0, Downloaded from https://rmets.onlinelibrary.wiley.com/doi/10.1002/qj.70215 by Lorenzo Giovannini - Universita Di Trento , Wiley Online Library on [07/05/2026]. See the Terms and Conditions (https://onlinelibrary.wiley.com/terms-and-conditions) on Wiley Online Library for rules of use; OA articles are governed by the applicable Creative Commons License

Drobinski, P., Bastin, S., Dusek, J., Zängl, G. & Flamant, P.H. (2006) Flow splitting at the bifurcation between two valleys: idealized simulations in comparison with mesoscale alpine programme observations. *Meteorology and Atmospheric Physics*, 92, 285–306. Available from: https://doi.org/10.1007/s00703-005-0158-3

Dudhia, J. (1989) Numerical study of convection observed during the winter monsoon experiment using a mesoscale two-dimensional model. *Journal of the Atmospheric Sciences*, 46, 3077–3107. Available from: https://doi.org/10.1175/1520-0469(1989)046<3077:NSOCOD>2.0.CO;2

Falocchi, M., Giovannini, L., de Franceschi, M. & Zardi, D. (2019) A method to determine the characteristic time-scales of quasi-isotropic surface-layer turbulence over complex terrain: a case-study in the Adige Valley (Italian Alps). *Quarterly Journal of the Royal Meteorological Society*, 145, 495–512. Available from: https://doi.org/10.1002/qj.3444

Falocchi, M., Tirler, W., Giovannini, L., Tomasi, E., Antonacci, G. & Zardi, D. (2020) A dataset of tracer concentrations and meteorological observations from the Bolzano tracer experiment (BTEX) to characterize pollutant dispersion processes in an alpine valley. *Earth System Science Data*, 12, 277–291. Available from: https://doi.org/10.5194/essd-12-277-2020

Flamant, C., Drobinski, P., Furger, M., Chimani, B., Tschannett, S., Steinacker, R. et al. (2006) Föohn/cold-pool interactions in the rhine valley during map iop 15. *Quarterly Journal of the Royal Meteorological Society*, 132, 3035–3058. Available from: https://doi.org/10.1256/qj.06.36

Giovannini, L., Antonacci, G., Zardi, D., Laiti, L. & Panziera, L. (2014) Sensitivity of simulated wind speed to spatial resolution over complex terrain. *Energy Procedia*, 59, 323–329. Available from: https://doi.org/10.1016/j.egypro.2014.10.384

Giovannini, L., Laiti, L., Serafin, S. & Zardi, D. (2017) The thermally driven diurnal wind system of the Adige valley in the Italian Alps. *Quarterly Journal of the Royal Meteorological Society*, 143, 2389–2402. Available from: https://doi.org/10.1002/qj.3092

Grell, G.A., Dudhia, J. & Stauffer, D. (1994) A description of the fifth-generation Penn State/NCAR mesoscale model (MM5). NCAR Scientific Tech Note, NCAR/TN-398+STR, 138. https://doi.org/10.5065/D60Z716B

Gucci, F., Giovannini, L., Stiperski, I., Zardi, D. & Vercauteren, N. (2023) Sources of anisotropy in the Reynolds stress tensor in the stable boundary layer. *Quarterly Journal of the Royal Meteorological Society*, 149, 277–299. Available from: https://doi.org/10.1002/qj.4407

Haid, M., Gohm, A., Umek, L., Ward, H.C., Muschinski, T., Lehner, L. et al. (2020) Foehn cold pool interactions in the inn valley during piano iop2. *Quarterly Journal of the Royal Meteorological Society*, 146, 1232–1263. Available from: https://doi.org/10.1002/qj.3735

Haid, M., Gohm, A., Umek, L., Ward, H.C. & Rotach, M.W. (2022) Cold-air pool processes in the inn valley during Föhn: a comparison of four cases during the PIANO campaign. *Boundary-Layer Meteorology*, 182, 335–362. Available from: https://doi.org/10.1007/s10546-021-00663-9

Hellström, R.Å., Fernández, A., Mark, B.G., Covert, J.M., Rapre, A.C. & Gomez, R.J. (2017) Incorporating autonomous sensors and climate modeling to gain insight into seasonal hydrometeorological processes within a tropical glacierized valley. *Annals of the American Association of Geographers*, 107, 260–273. Available from: https://doi.org/10.1080/24694452.2016.1232615

Hong, S.-Y. & Lim, J.-O.J. (2006) The WRF single-moment 6-class microphysics scheme (WSM6). *Asia-Pacific Journal of Atmospheric Sciences*, 42, 129–151.

Hong, S.-Y., Noh, Y. & Dudhia, J. (2006) A new vertical diffusion package with an explicit treatment of entrainment processes. *Monthly Weather Review*, 134, 2318–2341. Available from: https://doi.org/10.1175/MWR3199.1

Janjic, Z. (2002) Nonsingular implementation of the Mellor Yamada level 2.5 scheme in the NCEP Meso Model. *NCEP Office Note*, 436, 61.

Janjić, Z.I. (1994) The step-mountain eta coordinate model: further developments of the convection, viscous sublayer, and turbulence closure schemes. *Monthly Weather Review*, 122, 927–945. Available from: https://doi.org/10.1175/1520-0493(1994)122<0927:TSMECM>2.0.CO;2

Jaubert, G., Bougeault, P., Berger, H., Chimani, B., Flamant, C., Häberli, C. et al. (2005) Numerical simulation of meso-gamma scale features of föhn at ground level in the Rhine valley. *Quarterly Journal of the Royal Meteorological Society*, 131, 1339–1361. Available from: https://doi.org/10.1256/qj.03.197

Jiménez, M.A., Cuxart, J. & Martínez-Villagrasa, D. (2019) Influence of a valley exit jet on the nocturnal atmospheric boundary layer at the foothills of the Pyrenees. *Quarterly Journal of the Royal Meteorological Society*, 145, 356–375. Available from: https://doi.org/10.1002/qj.3437

Lampert, A., Pätzold, F., Jiménez, M.A., Lobitz, L., Martin, S., Lohmann, G. et al. (2016) A study of local turbulence and anisotropy during the afternoon and evening transition with an unmanned aerial system and mesoscale simulation. *Atmospheric Chemistry and Physics*, 16, 8009–8021. Available from: https://doi.org/10.5194/acp-16-8009-2016

Lapo, K., Dipankar, A. & Goger, B. (2025) Scale-aware evaluation of complex mountain boundary layer flow from observations and simulations. *Geophysical Research Letters*, 52, e2025GL116441. Available from: https://doi.org/10.1029/2025GL116441

Lareau, N., Crosman, E., Whiteman, C., Horel, J., Hoch, S., Brown, W. et al. (2013) The persistent cold-air pool study. *Bulletin of the American Meteorological Society*, 94, 51–63. Available from: https://doi.org/10.1175/BAMS-D-11-00255.1

Lareau, N.P. & Horel, J.D. (2015) Turbulent erosion of persistent cold-air pools: numerical simulations. *Journal of the Atmospheric Sciences*, 72, 1409–1427. Available from: https://doi.org/10.1175/JAS-D-14-0173.1

Lehner, M. & Rotach, M.W. (2018) Current challenges in understanding and predicting transport and exchange in the atmosphere over mountainous terrain. *Atmosphere*, 9, 276. Available from: https://doi.org/10.3390/atmos9070276

Lin, Y.-L., Reeves, H.D., Chen, S.-Y. & Chiao, S. (2005) Formation mechanisms for convection over the Ligurian sea during MAP IOP-8. *Monthly Weather Review*, 133, 2227–2245. Available from: https://doi.org/10.1175/MWR2970.1

Lundquist, J.D., Pepin, N. & Rochford, C. (2008) Automated algorithm for mapping regions of cold-air pooling in complex terrain. *Journal of Geophysical Research: Atmospheres*, 113, D22107. Available from: https://doi.org/10.1029/2008JD009879

Ma, M., Kang, G., Zhao, Z. & Cao, Y. (2024) Numerical simulation and its optimization of cold air pools in the Lanzhou Valley. *Meteorological Applications*, 31, e70020. Available from: https://doi.org/10.1002/met.70020

1477870x, 0, Downloaded from https://rmets.onlinelibrary.wiley.com/doi/10.1002/qj.70215 by Lorenzo Giovannini - Universita Di Trento , Wiley Online Library on [07/05/2026]. See the Terms and Conditions (https://onlinelibrary.wiley.com/terms-and-conditions) on Wiley Online Library for rules of use; OA articles are governed by the applicable Creative Commons License

Massey, J.D., Steenburgh, W.J., Knievel, J.C. & Cheng, W.Y.Y. (2016) Regional soil moisture biases and their influence on WRF model temperature forecasts over the intermountain west. *Weather and Forecasting*, 31, 197–216. Available from: https://doi.org/10.1175/WAF-D-15-0073.1

Mellor, G.L. (1982) Development of a turbulence closure model for geophysical fluid problems. *Reviews of Geophysics and Space Physics*, 20, 851–875. Available from: https://doi.org/10.1029/RG020i004p00851

Meybeck, M., Green, P. & Vörösmarty, C. (2001) A new typology for mountains and other relief classes: an application to global continental water resources and population distribution. *Mountain Research and Development*, 21, 34–45. Available from: https://doi.org/10.1659/0276-4741(2001)021[0034:ANTFMA]2.0.CO;2

Mlawer, E.J., Taubman, S.J., Brown, P.D., Iacono, M.J. & Clough, S.A. (1997) Radiative transfer for inhomogeneous atmospheres: RRTM, a validated correlated-k model for the longwave. *Journal of Geophysical Research Atmospheres*, 102, 16663–16682. Available from: https://doi.org/10.1029/97jd00237

Muñoz, R.C. & Armi, L. (2024) Hydraulic analysis and cold-air pool interaction of the raco gap wind. *Journal of Applied Meteorology and Climatology*, 63, 505–526. Available from: https://doi.org/10.1175/JAMC-D-23-0193.1

Muñoz, R.C., Armi, L., Rutllant, J.A., Falvey, M., Whiteman, C.D., Garreaud, R. et al. (2020) Raco wind at the exit of the maipo canyon in central chile: climatology, special observations, and possible mechanisms. *Journal of Applied Meteorology and Climatology*, 59, 725–749. Available from: https://doi.org/10.1175/JAMC-D-19

Neff, W.D. & King, C.W. (1987) Observations of complex-terrain flows using acoustic sounders: experiments, topography, and winds. *Boundary-Layer Meteorology*, 40, 363–392. Available from: https://doi.org/10.1007/BF00116103

Neff, W.D. & King, C.W. (1989) The accumulation and pooling of drainage flows in a large Basin. *Journal of Applied Meteorology*, 28, 518–529. Available from: https://doi.org/10.1175/1520-0450(1989)028<0518:TAAPOD>2.0.CO;2

Nikolic, J., Zhong, S., Pei, L., Bian, X., Heilman, W.E. & Charney, J.J. (2019) Sensitivity of low-level jets to land-use and land-cover change over the continental U.S. *Atmosphere*, 10, 174. Available from: https://doi.org/10.3390/atmos10040174

Niu, G.Y., Yang, Z.L., Mitchell, K.E., Chen, F., Ek, M.B., Barlage, M. et al. (2011) The community Noah land surface model with multiparameterization options (noah-MP): 1. model description and evaluation with local-scale measurements. *Journal of Geophysical Research Atmospheres*, 116, D12109. Available from: https://doi.org/10.1029/2010JD015139

Ookouchi, Y., Segal, M., Kessler, R.C. & Pielke, R.A. (1984) Evaluation of soil moisture effects on the generation and modification of mesoscale circulations. *Monthly Weather Review*, 112, 2281–2292. Available from: https://doi.org/10.1175/1520-0493(1984)112<2281:EOSMEO>2.0.CO;2

Pamperin, H. & Stilke, G. (1985) Nächtliche Grenzschicht und LLJ im Alpenvorland nahe dem Inntalausgang (Nocturnal boundary layer and low-level jet near the Inn Valley exit). *Meteorologische Rundschau*, 38, 145–156.

Pfister, L., Gohm, A., Kossmann, M., Wieser, A., Babić, N., Handwerker, J. et al. (2024) The teamx-PC22 alpine field campaign - objectives, instrumentation, and observed phenomena. *Meteorologische Zeitschrift*, 33, 199–228. Available from: https://doi.org/10.1127/metz/2024/1214

Pinto, J.O., Parsons, D.B., Brown, W.O.J., Cohn, S., Chamberlain, N. & Morley, B. (2006) Coevolution of down-valley flow and the nocturnal boundary layer in complex terrain. *Journal of Applied Meteorology and Climatology*, 45, 1429–1449. Available from: https://doi.org/10.1175/JAM2412.1

Price, J.D., Vosper, S., Brown, A., Ross, A., Clark, P., Davies, F. et al. (2011) Colpex: field and numerical studies over a region of small hills. *Bulletin of the American Meteorological Society*, 92, 1636–1650. Available from: https://doi.org/10.1175/2011BAMS3032.1

Rauchöcker, A., Rudolph, A., Stiperski, I. & Lehner, M. (2024) Cold-air pool development in a small alpine valley. *Quarterly Journal of the Royal Meteorological Society*, 150, 1243–1266. Available from: https://doi.org/10.1002/qj.4644

Reeves, D.H. & Lin, Y.-L. (2006) Effect of stable layer formation over the po valley on the development of convection during MAP IOP-8. *Journal of the Atmospheric Sciences*, 63, 2567–2584. Available from: https://doi.org/10.1175/JAS3759.1

Rucker, M., Banta, R.M. & Steyn, D.G. (2008) Along-valley structure of daytime thermally driven flows in the flows in the Wipp valley. *Journal of Applied Meteorology and Climatology*, 47, 733–751. Available from: https://doi.org/10.1175/2007JAMC1319.1

Sandu, I., Beljaars, A., Bechtold, P., Mauritsen, T. & Balsamo, G. (2013) Why is it so difficult to represent stably stratified conditions in numerical weather prediction (NWP) models? *Journal of Advances in Modeling Earth Systems*, 5, 117–133. Available from: https://doi.org/10.1002/jame.20013

Sasaki, K., Sawada, M., Ishii, S., Kanno, H., Mizutani, K., Aoki, T. et al. (2010) The temporal evolution and spatial structure of the local easterly wind 'Kiyokawa-dashi' in Japan Part II: numerical simulations. *Journal of the Meteorological Society of Japan*, 88, 161–181. Available from: https://doi.org/10.2151/jmsj.2010-204

Schmidli, J., Poulos, G.S., Daniels, M.H. & Chow, F.K. (2009) External influences on nocturnal thermally driven flows in a deep valley. *Journal of Applied Meteorology and Climatology*, 48, 3–23. Available from: https://doi.org/10.1175/2008JAMC1852.1

Skamarock, C., Klemp, B., Dudhia, J., Gill, O., Liu, Z., Berner, J. et al. (2019) A description of the advanced research WRF model version 4.

Spengler, T., Schween, J.H., Ablinger, M., Zängl, G. & Egger, J. (2009) Thermally driven flows at an asymmetric valley exit: observations and model studies at the Lech Valley exit. *Monthly Weather Review*, 137, 3437–3455. Available from: https://doi.org/10.1175/2009MWR2779.1

Stensrud, D.J. (1996) Importance of low-level jets to climate: a review. *Journal of Climate*, 9, 1698–1711. Available from: https://doi.org/10.1175/1520-0442(1996)009<1698:IOLLJT>2.0.CO;2

Svensson, N., Arnqvist, J., Bergström, H., Rutgersson, A. & Sahlée, E. (2019) Measurements and modelling of offshore wind profiles in a semi-enclosed sea. *Atmosphere*, 10, 194. Available from: https://doi.org/10.3390/atmos10040194

Therry, G. & Lacarrére, P. (1983) Improving the eddy kinetic energy model for planetary boundary layer description. *Boundary-Layer Meteorology*, 25, 63–88. Available from: https://doi.org/10.1007/BF00122098

Tomasi, E., Giovannini, L., Falocchi, M., Antonacci, G., Jiménez, P.A., Kosović, B. et al. (2019) Turbulence parameterizations

1477870x, 0, Downloaded from https://rmets.onlinelibrary.wiley.com/doi/10.1002/qj.70215 by Lorenzo Giovannini - Universita Di Trento , Wiley Online Library on [07/05/2026]. See the Terms and Conditions (https://onlinelibrary.wiley.com/terms-and-conditions) on Wiley Online Library for rules of use; OA articles are governed by the applicable Creative Commons License

for dispersion in sub–kilometer horizontally non-homogeneous flows. *Atmospheric Research*, 228, 122–136. Available from: https://doi.org/10.1016/j.atmosres.2019.05.018

Tomasi, E., Giovannini, L., Zardi, D. & de Franceschi, M. (2017) Optimization of Noah and Noah_MP WRF land surface schemes in snow–melting conditions over complex terrain. *Monthly Weather Review*, 145, 4727–4745. Available from: https://doi.org/10.1175/MWR-D-16-0408.1

Tuononen, M., O'Connor, E.J., Sinclair, V.A. & Vakkari, V. (2017) Low-Level Jets over Utö, Finland, based on Doppler Lidar observations. *Journal of Applied Meteorology and Climatology*, 56, 2577–2594. Available from: https://doi.org/10.1175/JAMC-D-16-0411.1

Umek, L., Gohm, A., Haid, M., Ward, H.C. & Rotach, M.W. (2021) Large-eddy simulation of foehn cold pool interactions in the inn valley during piano iop2. *Quarterly Journal of the Royal Meteorological Society*, 147, 944–982. Available from: https://doi.org/10.1002/qj.3954

Whiteman, C.D. (1990) Observations of thermally developed wind systems in mountainous terrain. In: *Atmospheric processes over complex terrain*. Boston, MA: American Meteorological Society, pp. 5–42.

Whiteman, C.D. & Doran, J.C. (1993) The relationship between overlying synoptic–scale flows and winds within a valley. *Journal of Applied Meteorology*, 32, 1669–1682. Available from: https://doi.org/10.1175/1520-0450(1993)032<1669:TRBOSS>2.0.CO;2

Whiteman, C.D., Zhong, S., Shaw, W.J., Hubbe, J.M., Bian, X. & Mittelstadt, J. (2001) Cold pools in the Columbia Basin. *Weather and Forecasting*, 16, 432–447. Available from: https://doi.org/10.1175/1520-0434(2001)0162.0.CO

Zängl, G. (2004) A reexamination of the valley wind system in the Alpine Inn Valley with numerical simulations. *Meteorology and Atmospheric Physics*, 87, 241–256. Available from: https://doi.org/10.1007/s00703-003-0056-5

Zardi, D., Falocchi, M., Giovannini, L., Tirler, W., Tomasi, E., Antonacci, G. et al. (2021) The Bolzano tracer experiment (BTEX). *Bulletin of the American Meteorological Society*, 102, E966–E989. Available from: https://doi.org/10.1175/BAMS-D-19-0024.1

Zardi, D. & Whiteman, C.D. (2013) Diurnal mountain wind systems. In: Chow, F.K., De Wekker, S.F. & Snyder, B.J. (Eds.) *Mountain weather research and forecasting: recent progress and current challenges*. Dordrecht: Springer Netherlands, pp. 35–119.

Zilitinkevich, S.S., Elperin, T., Kleeorin, N. & Rogachevskii, I. (2007) Energy–and flux–budget (EFB) turbulence closure model for stably stratified flows. Part I: steady–state, homogeneous regimes. *Boundary-Layer Meteorology*, 125, 167–191. Available from: https://doi.org/10.1007/s10546-007-9189-2

Zonato, A., Martilli, A., Jimenez, P.A., Dudhia, J., Zardi, D. & Giovannini, L. (2022) A new K–ϵ turbulence parameterization for mesoscale meteorological models. *Monthly Weather Review*, 150, 2157–2174. Available from: https://doi.org/10.1175/MWR-D-21-0299.1

How to cite this article: Gucci, F., Zonato, A., Falocchi, M., Zardi, D. & Giovannini, L. (2026) Observations and numerical simulations of a valley-exit wind in the Alpine Bolzano basin. *Quarterly Journal of the Royal Meteorological Society*, e70215. Available from: https://doi.org/10.1002/qj.70215

1477870x, 0, Downloaded from https://rmets.onlinelibrary.wiley.com/doi/10.1002/qj.70215 by Lorenzo Giovannini - Universita Di Trento , Wiley Online Library on [07/05/2026]. See the Terms and Conditions (https://onlinelibrary.wiley.com/terms-and-conditions) on Wiley Online Library for rules of use; OA articles are governed by the applicable Creative Commons License